CROSS SECTIONS FOR EXCITATION OF N_2^+ FIRST NEGATIVE AND MEINEL BANDS BY ELECTRON IMPACT

A

DISSERTATION

Presented to the Faculty of the

University of Alaska in Partial Fulfillment

of the Requirements

for the Degree of

DOCTOR OF PHILOSOPHY

by

ISHAQ MUHAMMAD MIRZA, B.Sc., M.Sc.

College, Alaska

May 1969

CROSS SECTIONS FOR EXCITATION OF N_2^+ FIRST NEGATIVE

AND MEINEL BANDS BY ELECTRON IMPACT

APPROVED:

Thomas D. Robert

Samuel B. Hawkins

Gerald J. Romick

John S Murray

B N Srivastava

Chairman

Thomas D. Robert

Department Head

APPROVED: C. Bullock DATE: Dec. 30, 1968

Dean of the College of Mathematics, Physical Sciences and Engineering

Vice President for Research and Advanced Study

ABSTRACT

The present study is important in interpreting visible and near-infrared auroral emissions in terms of electrons entering the atmosphere. The absolute excitation functions for the (0,0), (0,1) and (0,2) N_2^+ first negative bands and the (4,1), (2,0) and (3,1) N_2^+ Meinel bands produced by 0.07 - 4.0 keV electron impact have been measured.

The emission cross sections have been measured with a photon counting technique in a pressure range of 1.5 - 6.3 x 10^{-4} Torr in which the intensity of the radiation was proportional to both the electron current and the gas pressure.

The maximum emission cross sections for the (0,0), (0,1) and (0,2) N_2^+ first negative bands are 16.86 x 10^{-18} cm^2, 6.06 x 10^{-18} cm^2 and 1.16 x 10^{-18} cm^2 respectively, and for (4,1),(2,0) and (3,1) N_2^+ Meinel bands are 6.76 x 10^{-19} cm^2, 6.02 x 10^{-18} cm^2 and 2.35 x 10^{-18} cm^2 respectively, at 90-110 eV. The average ratio of the cross sections for the (0,0), (0,1) and (0,2) N_2^+ first negative bands is 1 : 0.34 : 0.065 and for the (2,0),(3,1) and (4,1) N_2^+ Meinel bands is 1 : 0.4 : 0.12. The apparent excitation cross section of the N_2^+ A $^2\Pi_u$ state is twice the apparent excitation cross section of the N_2^+ B $^2\Sigma_u^+$ state.

The excitation of the v'=0 vibrational level of the B $^2\Sigma_u^+$ state of N_2^+ is of the order of 0.1 of the total ionization cross section of N_2 by electron impact. This gives an energy flux of 60 ergs cm^{-2} sec^{-1} for the incident electrons in a type IBC III aurora.

The emission cross sections display an E^{-1} ln E dependence as described by the Bethe - Born approximation above 300 eV.

ACKNOWLEDGEMENTS

I wish to express my most sincere gratitude and thanks to Dr. S. N. Srivastava, Assistant Professor of Physics, under whose able guidance the present investigation was carried out.

I am indebted to many people at the Geophysical Institute and the Department of Physics for their help and assistance. Foremost among them are Professor A. E. Belon, Drs. C. S. Deehr, J. S. Murray, T. D. Roberts, G. J. Romick and J. R. Sheridan.

I am highly grateful to Professor Keith B. Mather, Director of the Geophysical Institute, for his constant encouragement and keen interest throughout this investigation and to Drs. T. D. Roberts and G. J. Romick for a critical reading of my original manuscript. I would also like to extend my appreciation to various technical groups at the Geophysical Institute, too numerous to be listed. Thanks are due Mr. C. H. Anderson for making the drawings and Mrs. M. McCoy and Mrs. B. J. Fossum for doing the tedious job of typing and preparing the final manuscript.

I wish to thank Dr. M. Rahmatullah, Director, Space Science and Research, Pakistan Space and Upper Atmosphere Research Committee, Karachi (Pakistan) for sending me abroad on their scholarship and the Atmospheric Sciences Section of the National Science Foundation Grant GA-920 for the financial support to carry out this work.

Finally, I thank my wife, Noor Jehan, for her extreme amount of patience and encouragement throughout this study.

TABLE OF CONTENTS

LIST OF TABLES

LIST OF FIGURES

LIST OF FIGURES (Cont'd)

CHAPTER I

INTRODUCTION

Available information (Chamberlain, 1961a) reveals that auroras can be excited by the bombardment of the upper atmosphere by the following particles:

1. Primary electrons and/or secondary electrons produced by the ionization of atmospheric gases by primary particles.
2. Energetic protons.
3. Hydrogen atoms produced by the neutralization of protons.

As these particles penetrate through the earth's atmosphere they undergo inelastic collisions (ionization, charge exchange, etc.) with atmospheric gases, leading in certain cases, to the excitations.

In order to find out which of these inelastic collisions will lead to the excitation of auroral lines and bands, it is necessary that one have knowledge of the following:

1. The rate of energy loss of electrons and protons through the atmosphere and the energy of these particles as they arrive at the auroral altitude.
2. The spectra of the atmospheric gases excited by bombarding particles having different energies.
3. The cross sections of different inelastic collisional processes between atmospheric gases and these particles.

Recent rocket and satellite measurements (O'Brien and Taylor, 1964; Evans and Belon, 1963) have demonstrated a good spatial and temporal

relationship between precipitated electrons and luminous auroras. The Belon, Romick and Rees (1966) study of the λ3914 N_2^+ first negative vertical luminosity profile indicated that the extreme energy values of auroral electrons are 0.7 to 6.0 keV but the main (characteristic) energy is between 1.0 and 4.0 keV. The study also indicated that electrons are the primary source for the production of negative bands. N_2^+ Meinel bands are also one of the prominent features in the infrared region, but studies of these bands are in a preliminary stage.

The energy flux of a beam of fast electrons absorbed by the atmosphere has been derived by Dalgarno et al. (1965) from the resulting intensity of the (0,0) λ3914 N_2^+ first negative band. The procedure is based upon the observation that the variation of the cross section for the production of λ3914 by electron impact with N_2 determined by McConkey and Latimer (1965) is very similar to that of the total ionization cross section and that the average energy loss per ion pair produced by an electron beam in nitrogen is constant at about 35 eV. Dalgarno et al. (1965) estimated an efficiency of 4.0×10^{-3} for the production of the λ3914 band by energetic electrons in the air, in fair agreement with the efficiency of 3.3×10^{-3} measured for 750 eV electrons by Hartman and Hoerlin (1962) [Hartman (1967) has recently repeated his measurement and obtained an efficiency of 3.4×10^{-3}].

The λ3914 cross section measured by McConkey and Latimer (1965) is higher than the earlier measurements of Stewart (1956), Sheridan et al. (1961), Hayakawa and Nishimura (1964), Davidson and O'Neil (1965) and Hayakawa et al. (1965) by a factor of 2 to 3 at the maximum.

Also, the curve falls off more sharply in the case of Stewart (1956) and Sheridan et al. (1961) at higher energies than McConkey and Latimer's (1965) curve.

Commenting on the note of Dalgarno et al.(1965), Davidson (1966) directed attention to the good agreement of the earlier cross section measurements [Stewart (1956), Sheridan et al. (1961), Hayakawa and Nishimura (1964) and Davidson and O'Neil, (1965)]. He pointed out that the data of McConkey and Latimer (1965) were taken with an indirectly calibrated system, while the earlier workers used standard lamp calibrations.

In view of such discrepancies it was desirable that the experiment be repeated from low energy to a few keV in order to cover the characteristic energy range for auroral electrons and to examine the validity of observations of Dalgarno et al. (1965). Work was in progress in our laboratory to measure the cross section for electron excitation of the N_2^+ Meinel band system. Concurrent with these measurements, the intensity of light emitted in the first negative bands was measured, and excitation cross sections were determined for electrons with energies of 70 eV to 2.5 keV. The measurement of λ3914, which was presented at the A.G.U. meeting [Srivastava and Mirza (1967)] was the first to provide direct support for the 'high' value of cross section reported by McConkey and Latimer (1965) in the energy range of threshold to 300 eV. Also, the measurements of Zapesochny and Skubenich (1966) for the $B\ ^2\Sigma_u^+$ state cross section provided indirect support for the higher cross section for the N_2^+ first negative bands.

In order to check the validity of the technique used by McConkey and Latimer (1965), McConkey, Woolsey and Burns (1967) measured the λ3914 cross section using a standard lamp calibration. They found good agreement with the values reported by McConkey and Latimer.

In our laboratory, the experiment to determine the slow electron excitation cross section of nitrogen bands in the visible and infrared region has been in progress since 1965-66. The present study includes the following measurements:

1. Measurements of the emission cross section for the N_2^+ Meinel [(4,1), (2,0); (3,1)] bands produced by the impact of electrons from 80 eV to 4.0 keV energy.
2. Measurements of the emission cross section for the N_2^+ first negative [(0,0), (0,1); (0,2)] bands in the energy range of 70 eV - 4.0 keV.

The choice of (4,1), (2,0) and (3,1) N_2^+ Meinel bands is made chiefly because of their importance in the auroral phenomena. These bands can be isolated from nearby first positive bands of N_2, while the other bands are completely or partially overlapped by the first positive bands. In appearance these bands are triple headed and degraded toward longer wave lengths. The exact wave lengths of the two (R_2 and Q_1) stronger band heads have been determined by Meinel (1951) and Douglas (1953). The stronger bands show, in addition, the presence of secondary maxima. The constants for these bands are known and thus all the relevant information for determining the absolute cross section by filter photometry is available.

No absolute excitation cross sections for the N_2^+ Meinel bands are available except for the total excitation cross section of the $A\ ^2\Pi_u$ state obtained by Zapesochny and Skubenich (1966) in a very limited energy range (threshold - 140 eV). Also, the measurements of Stewart (1955) for the (2,0) and (3,1) N_2^+ Meinel bands are only relative and have been done photographically in a very limited energy range (20 - 120 eV).

Because of the interest in a precise determination of the $\lambda 3914\text{Å}$ cross section (discussed earlier) and the non-availability of excitation cross sections for the $v' = 0$ progression of the N_2^+ first negative bands in the characteristic energy range of auroral electrons (1.0 to 4.0 keV), the experiment has been performed to determine these cross section.

The absolute emission cross sections for all the (0,0), (0,1) and (0,2) bands of the N_2^+ first negative system have been measured twice previously. [Stewart (1956), McConkey and Latimer (1965)]. Both the measurements of Stewart and McConkey and Latimer, are in a very limited energy range (25 - 300 eV). Not only are the cross sections of McConkey and Latimer (1965) a factor of 2 to 3 higher than Stewart (1956), but the measured relative intensities of the progression are in disagreement.

The measurements of the N_2^+ first negative and Meinel bands cross section will provide data to stimulate and test the development of semiclassical theories which rely heavily on the availability of

experimental data in the absence of any quantum mechanical predictions for heavier gases.

The details of experimental arrangement, calibration techniques and results with a concluding discussion are presented in subsequent chapters.

CHAPTER II

EXPERIMENTAL APPARATUS

2.1 General Description

The schematic diagram of the experimental arrangement is shown in Figure 1. The radiation studied was produced by a well defined electron beam. The fast electron beam passed through a low pressure gas cell target and the light emitted from the beam path was studied at right angles to the beam direction through a quartz window and interference filters. During the experiment, the pressure of the electron gun chamber was kept at about 10^{-6} Torr to avoid contamination of the gun. The pressure inside the collision chamber was varied from 6.3×10^{-4} to 1.5×10^{-4} Torr during the observations. The electron energy was varied from 70 eV to 4 keV. The electron currents were usually from 2.5 μA to 25 μA. Single photon counting techniques were used in the present investigation. However, in the beginning some measurements were made by the d.c. technique (i.e. the beam current and the photometer output were simultaneously measured by d.c. electrometers). In all the observations the anisotropy of the emitted radiation was evaluated.

2.2 Vacuum System

The vacuum system consists of the usual type of diffusion pump backed up by a mechanical pump. The diffusion pump is an oil-type 2" CVC "Blueline" which has a plateau pumping speed of 104 liters per second and a back streaming rate of 0.3 cc per hour. The main system is connected to the diffusion pump through freon refrigerated and air

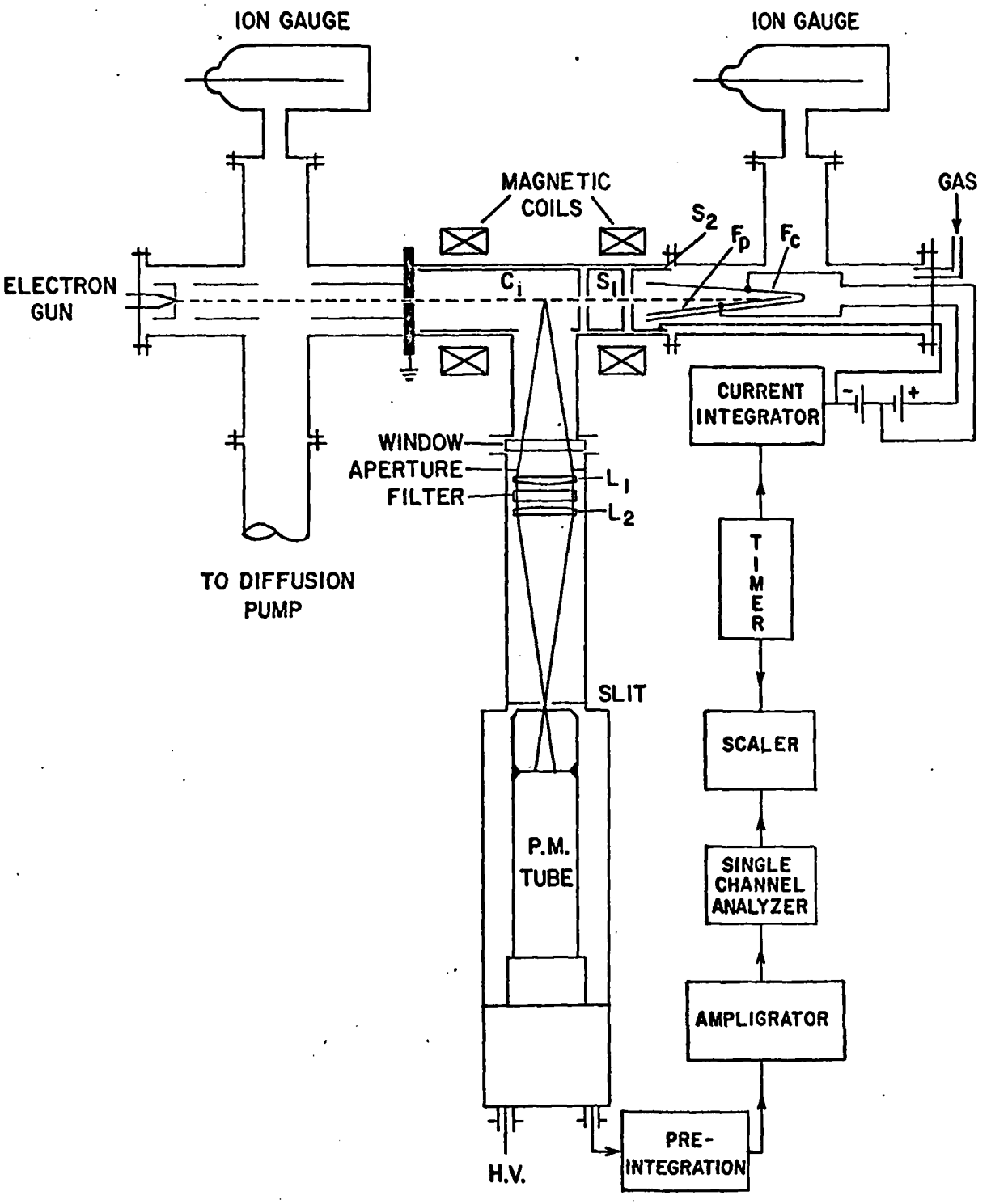

Figure 1 Schematic view of the apparatus used for measuring the emission cross sections.

cooled baffles to avoid back streaming of diffusion pump oil into the system.

The mechanical pump is a Welch two stage "Duo-Seal" rotary oil pump Model No. 1402 which has a pumping rate of 140 liters free air per minute. The gate, the fore and the roughing valves used in the vacuum system are pneumatically operated. The various valves and the diffusion pump are interlocked so that the diffusion pump and gate valve shut off automatically if a leak develops in the system or if the water supply used to cool the diffusion pump is interrupted. The interlocking system provides a facility for continuous evacuation of the system without danger of diffusion pump oil entering into the system.

The vacuum vessels (main system) consist of 2" Pyrex glass pipes which are joined by neoprene gaskets using high vacuum silicone grease. The various vacuum system components are joined together by 2.2 cm copper tubing. Once the vacuum seals are made and the system is outgassed, it is very easy to obtain a pressure of 10^{-7} Torr. The pressure of the system is recorded by two Veeco RG 75 ionization gauges. The pressure readings of these gauges are calibrated against a high vacuum McLeod Gauge (calibration is discussed further in Chapter IV).

2.3 Electron Gun

A schematic diagram of the electron gun is shown in Figure 2. The filament is a hair pin V-shaped thoriated-tungsten wire F across which an a.c. voltage (1.0 - 1.5 V) is applied through a filament transformer.

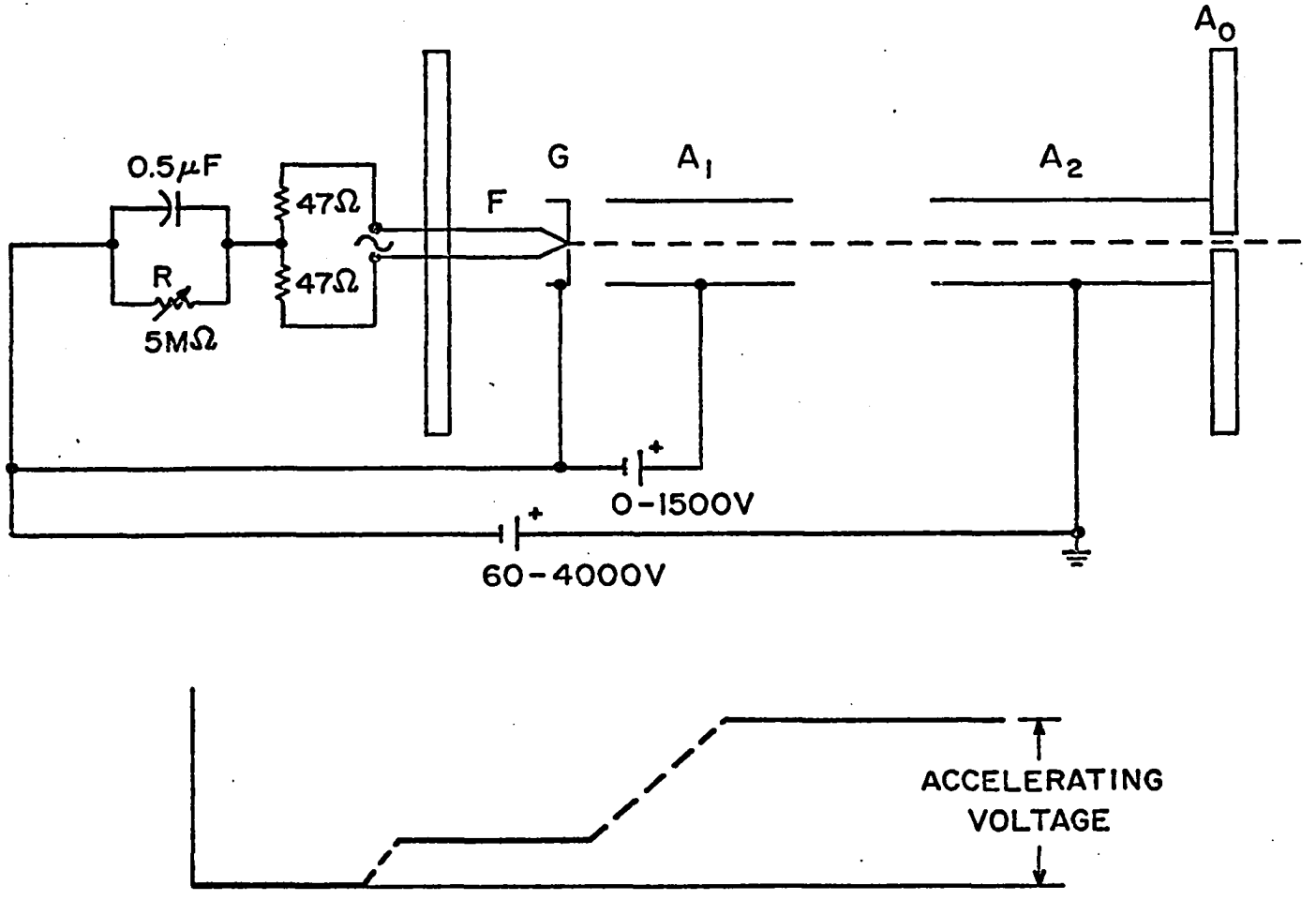

Figure 2 Electron gun assembly.

The primary voltage to the filament transformer is provided by a variac. The grid G is biased a few volts negative with respect to the filament by adjusting the resistor R. This type of grid biasing avoids overloading of the filament. A_1 and A_2 are two cylindrical electrodes made of 2.5 cm diameter aluminum tubing and are 5.1 cm and 7.6 cm long respectively. A_o is a 6.4 mm thick aluminum plate having a 3.2 mm beam defining aperture in the center. This also maintains a differential pressure between the gun and the collision chamber sections. The electrode A_2 and the plate A_o are connected together and are kept at ground potential. The potential to A_2 (final accelerating voltage) is supplied by a John Fluke High Voltage Power Supply Model No. 408A (0.5 to 6.0 kV) and the potential to electrode A_1 is supplied by a Northeast Scientific Corporation Regulated High Voltage Supply Model No. ZRE 1603 (0 to 1.6 kV). Potentials along the beam path are shown in Figure 2.

2.4 Focusing

The three cylindrical electrodes A_2, A_o and G form an electrostatic lens system. The building up of a space charge is eliminated by the negative biasing of grid G. Electrode A_1 serves as the first accelerating anode and A_2 serves the final accelerating anode. The potential applied to electrode A_2 is always kept greater than the potential at A_1. The potential at A_2 is taken as the final energy of the electrons. A well-defined narrow beam of electrons is passed into the collision chamber through the aperture of plate A_o. In order to overcome the

deflection of the beam due to the earth's magnetic field (0.6G), a permanent bar magnet is placed outside the electron gun assembly and its position is adjusted in order to obtain a straight beam along the axis of the collision chamber. The divergence of the beam is suppressed by the two axial magnetic coils wound around the collision chamber as shown in Figure 1. By adjusting the potential on electrode A_1, the grid biasing, the filament voltage, the bar magnet position and the strength of the axial magnetic field, a well-defined and collimated beam of electrons is obtained in the energy range of 70 eV - 4 keV.

2.5 Beam Collection

The collision chamber along with the beam collecting system is shown in Figure 3. The electron beam enters into the collision chamber through the beam defining aperture of the plate A_o. C_1, S_1 and S_2 are three 4.7 cm diameter aluminum cylinders. C_1 is the collision chamber which is described in detail in the next section. S_1 and S_2 are two shields which are kept at ground potential. The apertures in the shields are 0.48 cm in diameter. The electron collector assembly consists of three elements, S_2, F_c, and F_p. The Faraday cage F_c is a wedge-shaped 15.2 cm long collector made of copper plates as shown in Figure 4. [In the preliminary stage of the work an ordinary type of Faraday cup was used.] The plate F_p is insulated from F_c by two teflon spacers. F_p and F_c are biased 135 - 180 volts and 45 - 90 volts, respectively, positive with respect to the shield S_2. The wedge-shaped design of the cage prevents the reflection of electrons, and the escape

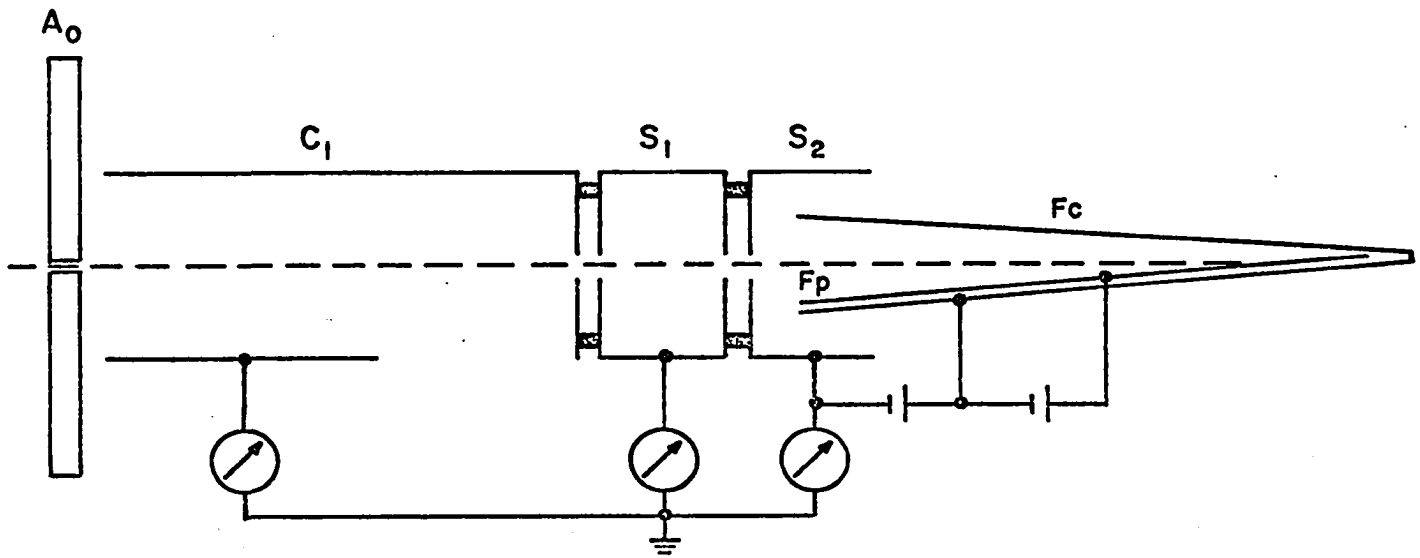

Figure 3 Schematic view of the collision chamber, shields and the beam collector assembly.

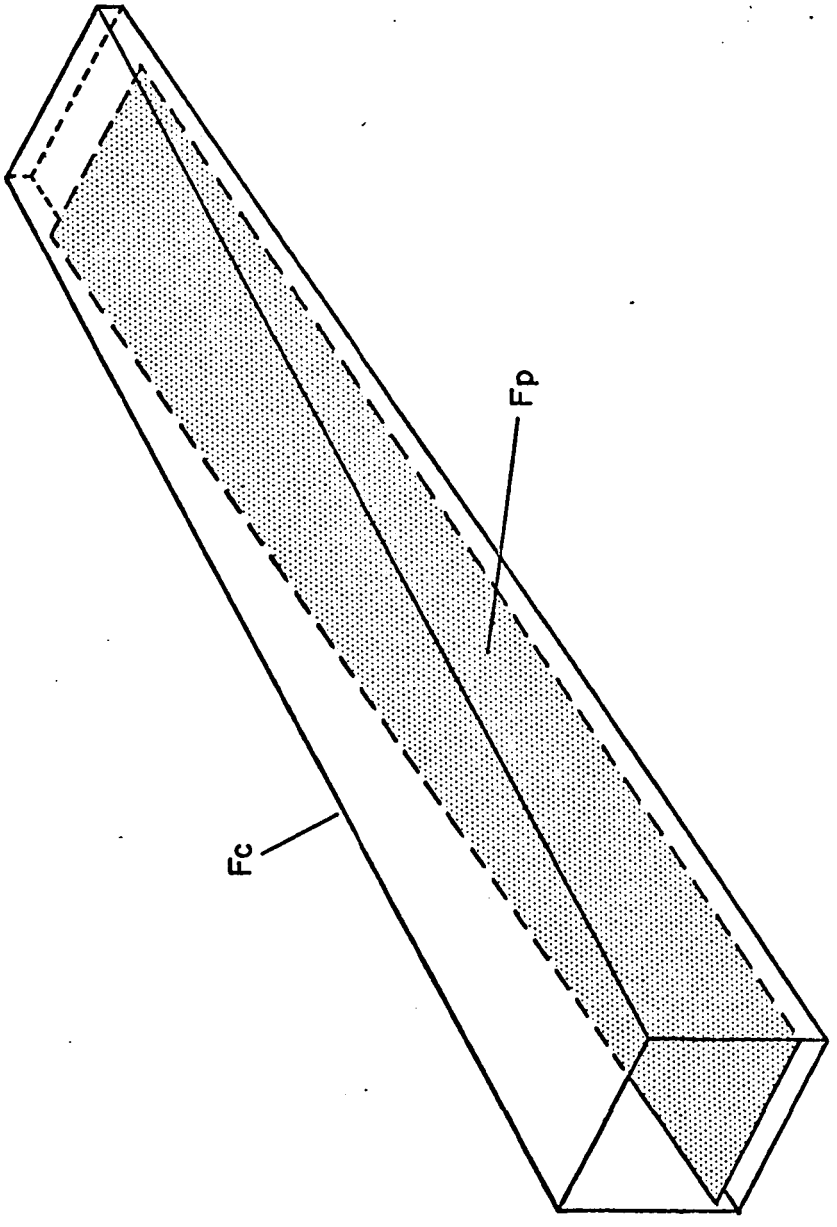

Figure 4 Faraday cage.

of secondary electrons from the collector assembly. The shield S_1 prevents the penetration of the positive field from the collector assembly into the collision chamber and also helps to collimate the beam.

2.6 Collision Chamber

Essentially the collision chamber consists of an aluminum cylinder C_1 which is 12.7 cm long and 4.7 cm in diameter enclosed in a tee-shaped pyrex glass envelope. One side of the collision chamber (facing the shield S_1) is closed by a thin aluminum plate having a circular aperture of 0.8 cm. Near the closed end of the cylinder is a 5.1 x 2.5 cm rectangular window through which the radiation is viewed at right angles to the beam direction. The inside of the collision chamber assembly is painted with acquadag to prevent any reflection of light from its walls. The collision chamber is grounded to avoid the effects of any stray electrical fields and the building up of an electrostatic charge. The optical window is made of a 1.3 cm thick and 6.3 cm diameter circular quartz slab which is flanged to one limb of the Pyrex-Tee facing the rectangular window of the collision chamber C_1.

2.7 Beam Collimator

The collimator is 16.4 cm long barrel with a 4.7 cm inside diameter. It is made from an aluminum cylinder with a wall thickness of 1.0 cm and houses an aperture, 2 lenses, an interference filter and a slit. The geometrical arrangement of various optical components is shown in Figure 5.

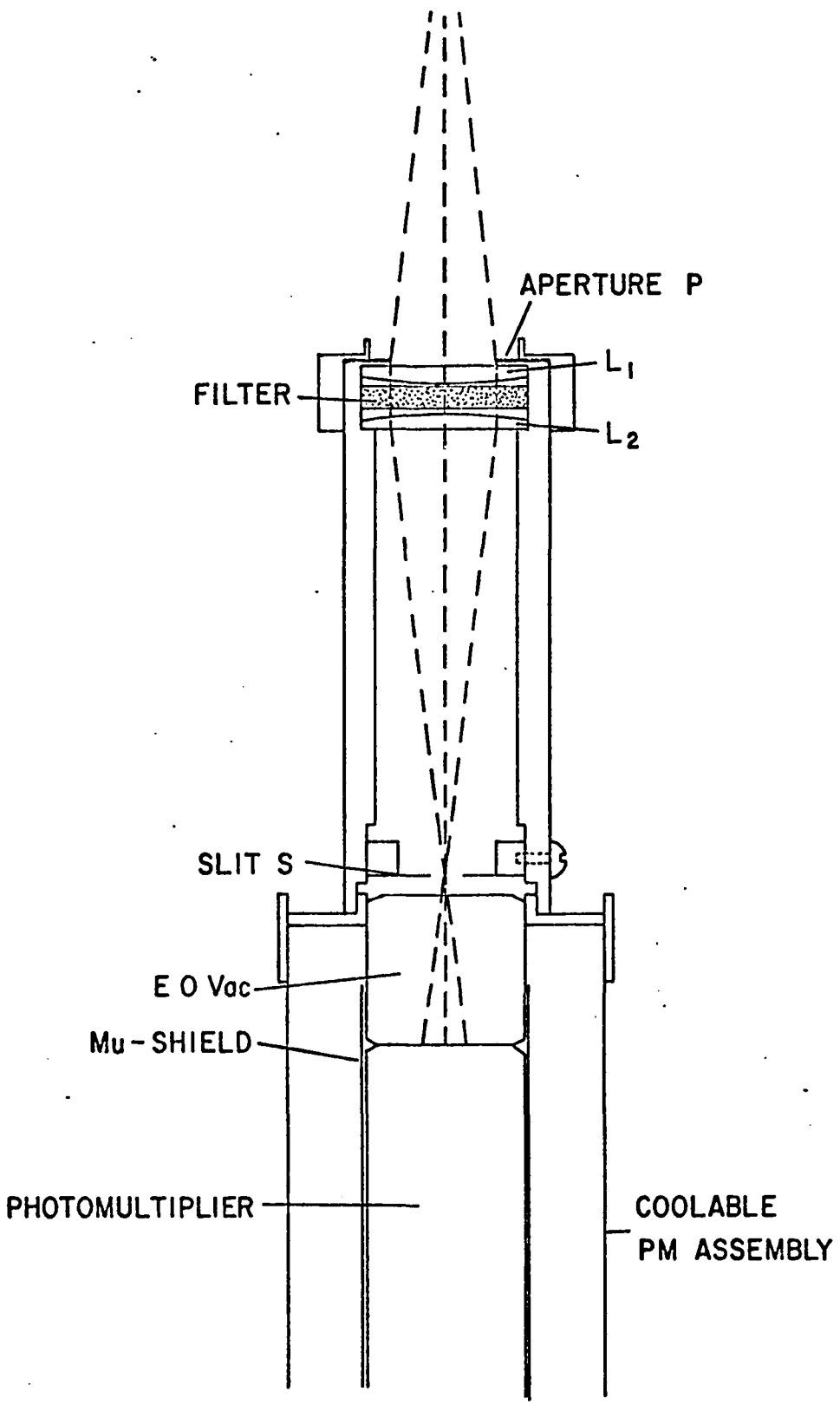

Figure 5 Collimator system and photometer.

P is an aperture which defines the solid angle of radiation seen by the photometer. L_1 and L_2 are two 4.9 cm plano-convex lenses used for the collimation. The focal lengths of the two lenses L_1 and L_2 are 14.6 cm and 12.7 cm respectively. The distance between the first lens L_1 and the center of the electron beam is equal to its focal length (14.6 cm). A parallel beam of light emerging through lens L_1 passes normal to the interference filter and is finally focused by the lens L_2 on slit S. The slit S can be adjusted to select the desired beam length for the observations. During most of the experiment it was set at 1.0 cm. The magnification of the lens system is 0.87 and therefore the actual beam length observed was 1.15 cm. The light coming through the slit falls on the photocathode of the photomultiplier tube traversing an "EOVac" seal whose function is described in the Photometer Section. In this arrangement the maximum angle of incidence at the interference filter is within 2°. This assures that the normal incidence characteristics of the filter have not changed during the observation. A thin circular polarizer can be installed between the aperture P and the quartz window to determine the amount of polarization in the irradiated light. Details of the polarization measurement are discussed in Chapter IV.

2.8 Photometers

For measurement of the small light intensities encountered in the collisional excitation experiments, a careful selection of the photomultiplier tube is necessary. The major limitation is the dark current

and the fluctuations associated with it. Various causes of the dark current are discussed in a manual of the "Dark Current in Photomultiplier Tubes" from E.M.I. Electronics Ltd., but two of these causes are the most fundamental and important. These are the thermionic emission of the dynode system, and the photocathode and fluorescence of the photomultiplier walls.

According to ideal statistics, the average fluctuation in the number of thermionic electrons emitted in a given time is equal to $(N_d)^{\frac{1}{2}}$ where N_d is the total number of thermionic electrons emitted in that time. Proper selection and cooling of the photocathode material can reduce considerably the number of thermionic electrons and hence the fluctuation. Furthermore, the dark current fluctuations can be reduced by using an appropriate signal detection system which is described in the next section.

The fluorescence of the walls of the photomultiplier tube is prevented by operating the tube with its cathode and the outer wall at the same potential.

Again, from ideal statistics, the Signal to Noise ratio is given by

$$S/_N = \dot{N}_p \, q \, (e \cdot g \cdot \frac{t}{i_d})^{\frac{1}{2}}, \qquad 2.1$$

where $\dot{N}_p$ is the number of photons striking the photocathode surface per sec , q is the quantum yield ratio, e is the electronic charge, g is the current gain of the photomultiplier, i_d is the dark current detected at the anode and t is the time interval over which the anode

pulses are collected. The quantities which depend directly upon the type of photomultiplier tube are g, q and i_d.

Another important factor is the area of the photocathode. A larger area would allow a larger beam length to be studied and hence would increase the current output of the photometer.

With all the above considerations in mind the RCA 7265 and the Amperex 56CVP photomultipliers were selected to cover the entire region of intended observations. The two tubes are manufacturer's "Select-Type" (having higher sensitivites and lower dark currents than the average type tube). The RCA 7265 with an S-20 photocathode surface was used in the region 3800 Å to 7900 Å and the Amperex 56CVP with an S-1 cathode surface was used for the λ8080 (3,1) N_2^+ Meinel band.

A coolable Photomultiplier Assembly Model PM-102 of Electro-Optics Associates was used for housing the photomultiplier tubes. To prevent frosting and fogging of the tubes, specially made vacuum seals called "EOVac" were epoxied to both of the tubes. The RCA 7265 photomultiplier tube was operated at room temperature to record the strong N_2^+ first negative bands while for the two N_2^+ Meinel bands [(4,1) and (2,0)] the tube was cooled by cold dry air passing through a freezing mixture. The Amperex 56 CVP was cooled by dry ice for observation of the (3,1) N_2^+ Meinel band.

A mu-metal shield was placed around the photomultiplier tubes to prevent any distortion in the function of the dynode system due to any stray electric and magnetic fields. By keeping it at the photocathode's potential, the fluorescence of the tube walls was also prevented.

2.9 Signal Detection Apparatus

Two different methods were employed for the detection of the signals. In the earlier part of the studies, mainly due to lack of funds, a d.c. current integrating procedure was used. Both the beam current and output of the photometer were measured by 600A and 610A Keithly Electrometers. Later on, a beam integrator and a photon counting system were set up.

The chief advantage in using the photon counting technique over the d.c. method is that by selecting the proper base line of the single channel analyzer, the smaller pulses due to the thermionic emission from the various dynodes can be discriminated against the larger pulses produced at the photocathodes. This improves the S/N ratio considerably. Furthermore, by integrating the beam current and the output pulses of the photometers, the fluctuation in the beam intensity is also accounted for.

The block diagram of the signal detection system is shown in Figure 1. A Current Indicator and Integrator Model No. A 309C manufactured by Elcor is used to integrate the beam current over a desired period of time. The Ampligrator (Amplifier and Integrator), the Single Channel Analyzer, the Electronic Timer and the Scaler are made by Elron.

The Ampligrator Model CA-N-262 is a current-operated module and is desired for use in high resolution spectroscopy. Its charge collection time is 1.0 n sec to 12.0 μsec and the current gain is from 16 to 16,000. The integrating time constants are from 0.1 to 12.8 μsec; the intrinsic rise-time is less than 30 n sec. Its amplifier pass-band at low frequency is 3 db down at 15 cycles per sec.

The Model SCTD-N-10X Precision Single Channel Analyzer is also a current-operated module. Its resolving time is less than 0.7 μsec and the rise time of accepted signals is less than 0.25 μsec.

The Electronic Scaler Model No. NIS-17 has a Nixie display with a count capacity of 7 digits. Its counting accuracy is absolute, the resolution is better than 0.7 μsec to pulse pairs and the maximum counting rate is 1.5 million counts per sec.

A Dual Purpose Electronic Recycle Timer Model TI-N-100B is used as a master switch to stop the scaler and the beam integrator unit simultaneously, after a preset length of integration period. Typically, an integration time of 50 seconds was used.

CHAPTER III

EXPERIMENTAL PROCEDURE

The entire vacuum system is evacuated continuously for several weeks. After a careful degassing of the glass chambers and other components with a heat gun, the typical pressures obtained are 7 x 10^{-7} Torr in the gun chamber and 2 x 10^{-5} Torr in the collision chamber section. After the long evacuation, prepurified nitrogen gas of purity 99.9% manufactured by Industrial Air Products is introduced through a variable leak valve at a relatively high pressure ($\sim$ 30 milli Torr) for about half an hour. After flushing the system, the pressure in the collision chamber is reduced to the desired value ($\sim$ 5 x 10^{-4} Torr) and the system is allowed to run for several more days to achieve equilibrium. Pressure readings of the ion gauges are taken throughout this period. A constant reading of the collision chamber's pressure is indicative of the equilibrium conditions, after which the observations could be started.

3.1 N_2 Molecular Spectra Excited by Electrons

Various scans of the optical spectrum from λ3000 Å to λ8000 Å with different electron energies and gas pressures were made in the first order of a 70 cm f/3.4 Ebert-Fastie Spectrograph which was designed by the author and built locally. The appearance of the first negative emissions in the second order of the grating prohibited the identification of the Meinel bands. A yellow filter

having a cut off at about 6000 Å was used to isolate the presence of second order emissions. Two typical scans with and without the filter are shown in Figure 6.

3.2 Beam Current and Pressure

The variation of the emitted light intensity per incident particle as a function of the target gas pressure p is important since it is used as a criterion to determine the source of optical emission. If the emissions are due to the collisions between the primary incident particles and the target gas, the light intensity per incident particle will be a linear function of p. However, if there are some secondary processes present, the dependence will be quadratic.

In order to verify the single collision condition, linearity of the photometer's output, both with the gas pressure and the beam current, was checked and is shown in Figure 7 for both the first negative and Meinel bands. The intensities of the first negative and the Meinel bands are proportional to the gas pressure as well as to the beam current below a pressure of 1m Torr. In all the observations, collision chamber pressure was kept much lower than 1m Torr. The actual gas pressure inside the collision chamber during the observations for various bands are listed in Table 1.

3.3 Data Taking Procedure

The pressure inside the collision chamber is recorded by the ion gauge. The narrow band pass interference filter for a particular band to be studied is placed in the collimator which is then mounted on the

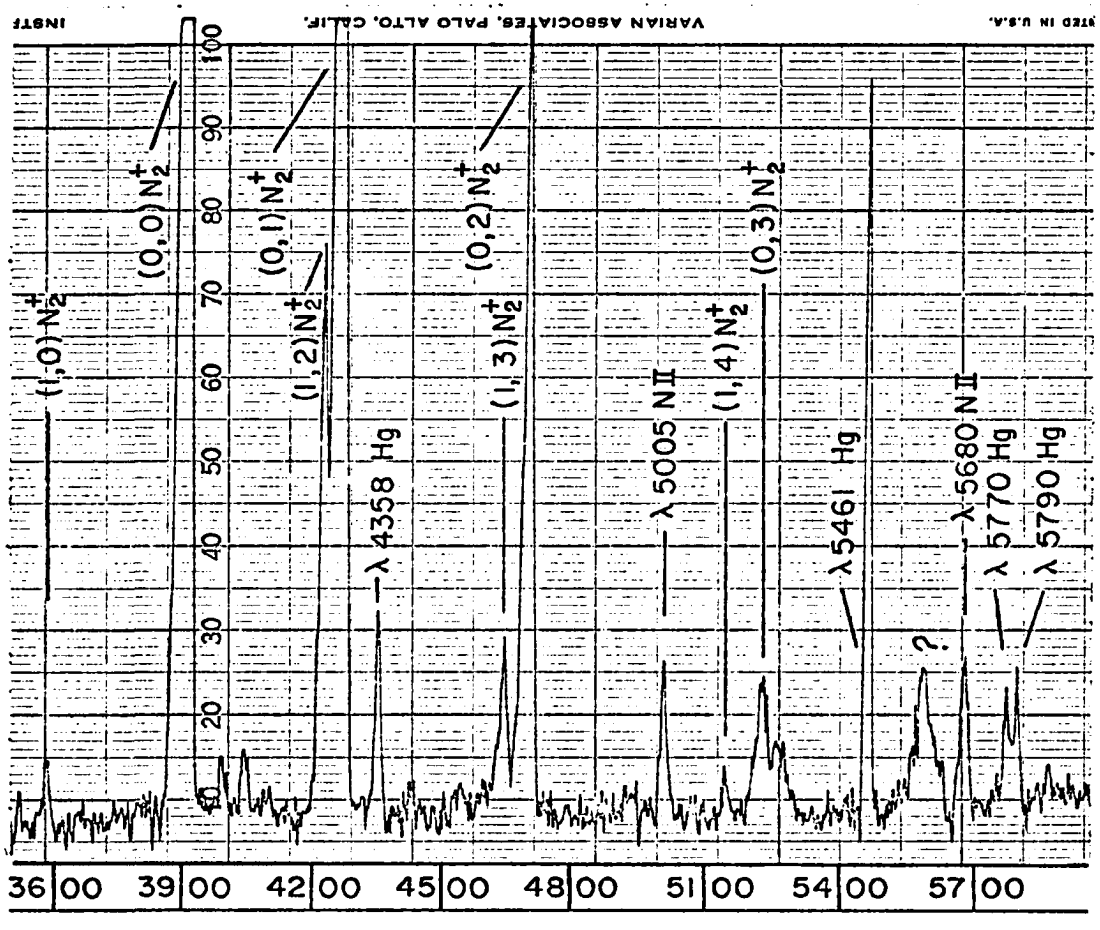

Figure 6 N_2 molecular spectra excited by 500 eV electrons (16 Å resolution) along with mercury lines.

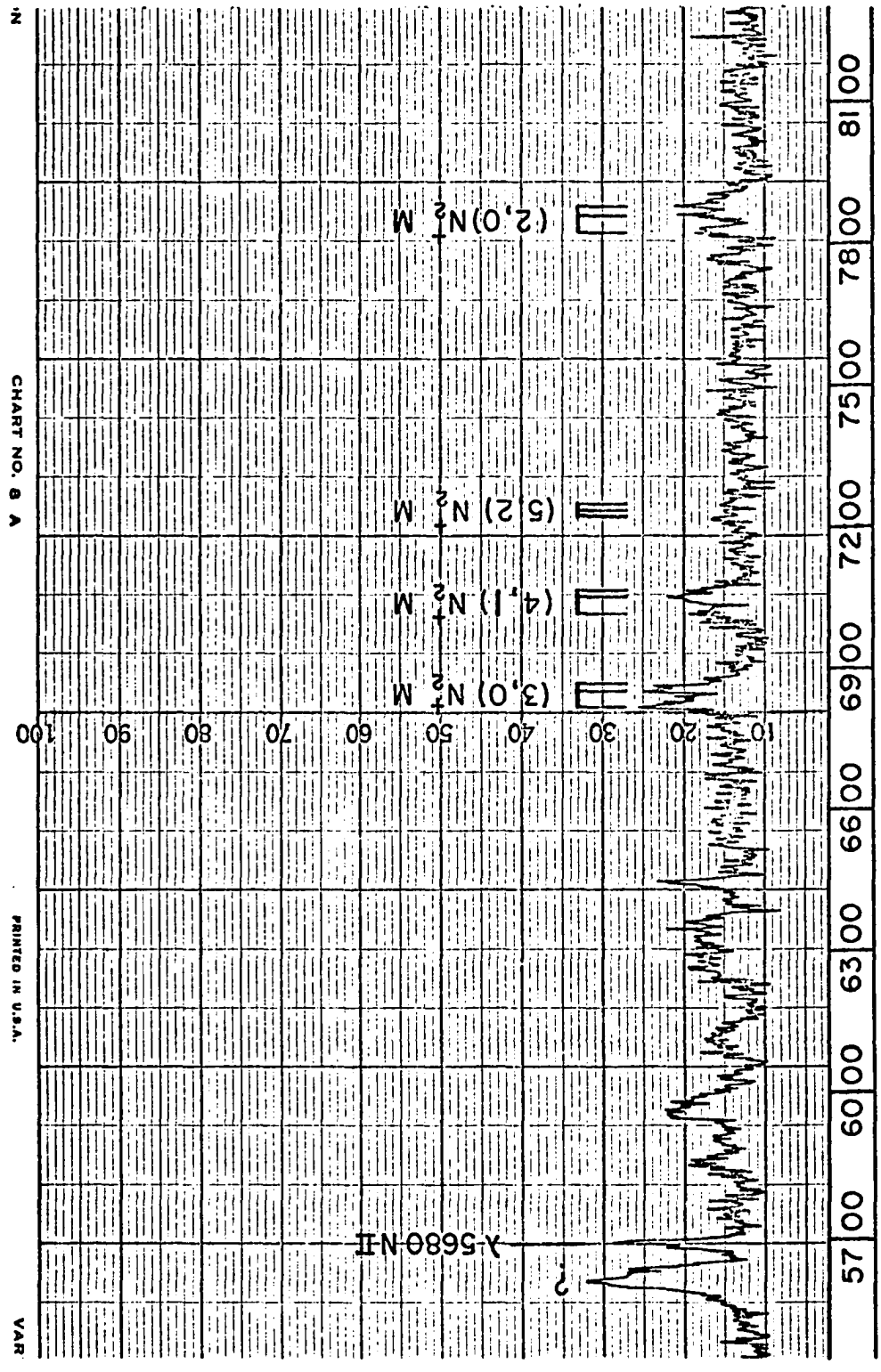

Figure 6 continued

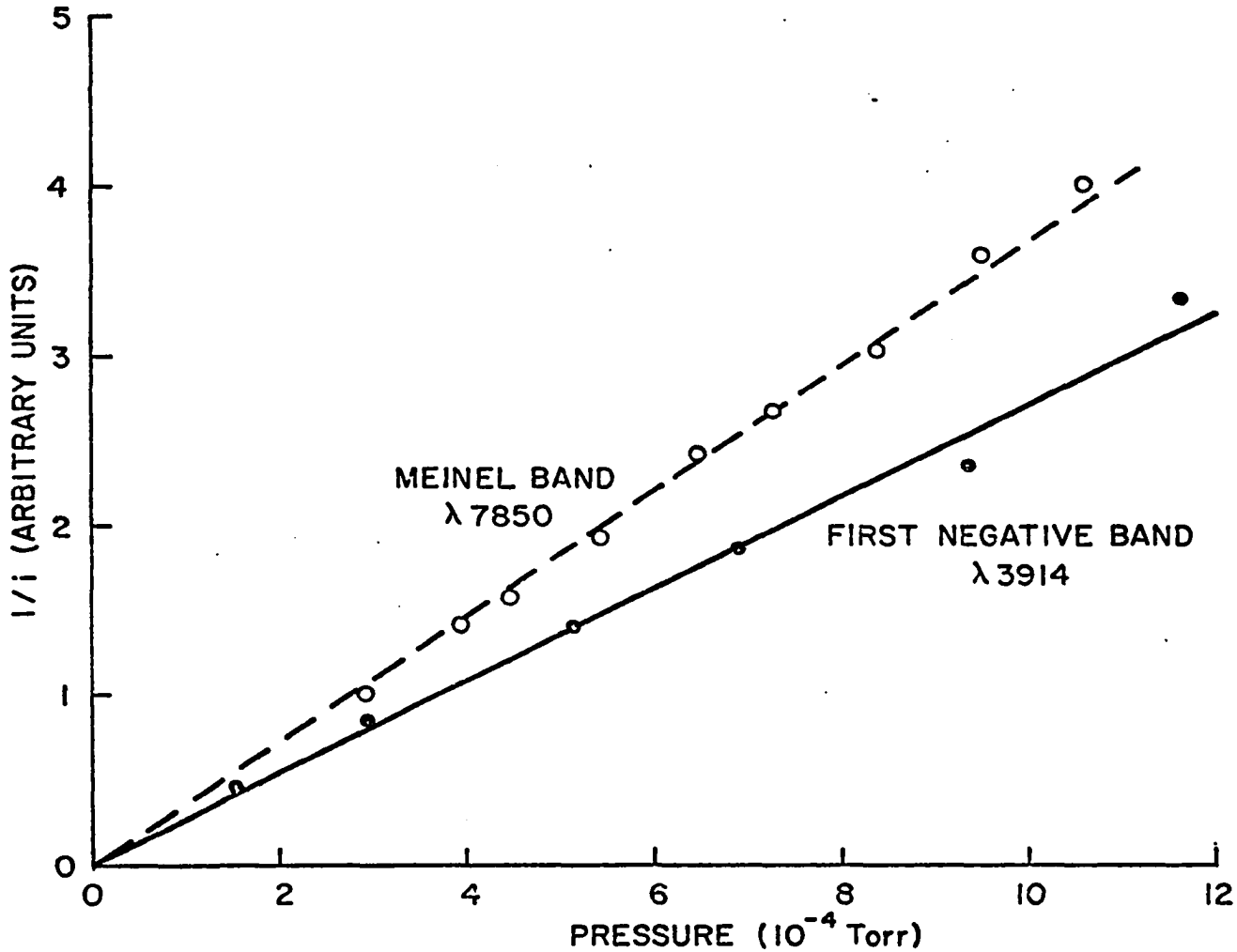

Figure 7 N_2^+ bands radiation per unit beam current versus the target gas pressure.

TABLE 1

Target Gas Pressure Inside the Collision Chamber During Observation

Band	Pressure (x 10^{-4}) Torr
First Negative	
3914 (0,0)	2.0
4278 (0,1)	1.5
4709 (0,2)	3.0
Meinel System	
7059 (4,1)	2.0
7850 (2,0)	6.3
8080 (3,1)	5.9

quartz window (see Figure 1). The potential at the anode A_2 (Figure 2) is set at the desired value of beam energy (70 eV - 4.0 keV). The filament voltage, the resistance R, the position of the bar magnet and the voltage of A_1 are adjusted to get a beam current of a few microamperes. The beam is usually well collimated in the collision chamber after entering through the aperture A_o and can be seen by the naked eye. It starts diverging slightly at the other end of the collision chamber. A variable axial magnetic field (up to 250 G) is used to further collimate the electron beam. Electron currents at the collision chamber C_1 and shield S_1 are also monitored to check the beam collimation. The sum of the currents at the collision chamber C_1 and Shield S_1 during the observation is always less than 1% of the total beam current up to 2.0 keV and less than 1.5% up to 4.0 keV.

The current at the shield S_1 which is a part of the electron beam exciting the observed radiation is added to the total beam current measured at the collector assembly consisting of S_2, F_c and F_p (see Figure 3). The electron current at the collision chamber C_1 was always less than 0.5% of the total beam current and was neglected in deducing the cross section.

The pulse output of the photometer is preintegrated by an RC integration circuit (Time constant = 2.4×10^{-7} sec) before going through the linear amplifier. The amplified pulses are counted on the scaler after passing through the discriminator. The discriminator base line is so adjusted that the smaller pulses from different dynodes are suppressed and the signal/noise ratio is greatest. Both the current

integrator and the scaler are programmed by the relay system of the electronic timer which stops them automatically after a fixed time of integration. Several data points ($\sim$ 10) are taken for a particular electron energy and their mean value has been used for deducing the cross section. The maximum scatter of the data points is less than 5%. Also day-to-day reproduction is better than 5%.

After completion of the observations of a particular electron energy the potential at A_2 is changed to the next desired electron energy. The same procedure is repeated for the entire energy range. Pressure readings are taken during each set of observations. The maximum fluctuation in the pressure readings is always less than 1%.

CHAPTER IV

PROCEDURE OF DATA REDUCTION

The present experiment is concerned with the following inelastic collision of an electron with N_2 molecules.

$$N_2 \, (X \, {}^1\Sigma_g^+)_{v=0} + e \rightarrow N_2^+ \, (A \, {}^2\Pi_u \text{ or } B \, {}^2\Sigma_u^+)_{v'} + e + e' \text{ (excitation)} , \quad (4.1)$$

and

$$N_2^+ \, (A \, {}^2\Pi_u)_{v'} \rightarrow N_2^+ \, (X \, {}^2\Sigma_g^+)_{v''} + h \, \nu_{v'v''} \quad \text{(Meinel band emission)} , \quad (4.2)$$

or

$$N_2^+ \, (B \, {}^2\Sigma_u^+)_{v'} \rightarrow N_2^+ \, (X \, {}^2\Sigma_g^+)_{v''} + h \, \nu_{v'v''} \text{ (First Negative band emission)} , \quad (4.3)$$

where $\nu_{v'v''}$ is the frequency of the radiation recorded due to the vibrational transition from the v' level of $A \, {}^2\Pi_u$ or $B \, {}^2\Sigma_u^+$ states to the v'' vibrational level of $X \, {}^2\Sigma_g^+$ state.

In order to determine the absolute emission cross section, it is essential that in any experimental set up, the errors due to the anisotropy of the emitted radiation, pressure measurement and photometric calibration should be properly analyzed and estimated.

Working with the assumption that the upper states of the N_2^+ first negative and Meinel bands are excited by the simultaneous ionization and excitation from the ground state of N_2 by electron impact, the frequencies of the lines of a particular band and their relative intensities are calculated to determine the filter factor (effective

transmission coefficient) of the interference filter used for recording the emission of that band.

4.1 Theory of the Experiment

As mentioned above, in the present experiment an electron beam is injected into a collision chamber filled with nitrogen gas. The passage of the beam through the target gas forms excited particles which, with the exception of metastable states (if any), decay with the emission of radiation. The absolute measurement of the intensity of certain emission gives the rate of population of a particular excited state and hence, in principle, the cross section σ for the formation of that state. An excited state, j, may be populated directly by excitation from the ground state or by cascade transition from a higher state, i. Depopulation of state j takes place by radiative transmissions to state k, lying below j. The time rate of change of the population of molecules in the excited state j in one cm of beam path can be written as

$$\frac{dN_j}{dt} = \sigma_j \frac{I}{e} N_o - \sum_k A_{jk} N_j + \sum_i A_{ij} N_i \quad , \tag{4.4}$$

where N_j and N_i are, respectively, the number of particles in state j and i produced per cm of beam path, A_{jk} and A_{ij} are the probabilities per second of spontaneous radiative decay in the transition $j \rightarrow k$ and $i \rightarrow j$, respectively, N_o is the number of target particles per cm^3, σ_j is the excitation cross section of the j states in cm^2, I is the electron beam current and e is the electronic charge. Therefore, I/e is the

number of incident electrons per second.

After equilibrium has been established, the density N_j of the excited molecular ions is constant and therefore equation (4.4) is reduced to

$$\sigma_j \frac{I}{e} N_o = \sum_k A_{jk} N_j - \sum_j A_{ij} N_i \quad . \tag{4.5}$$

It is convenient to define an emission cross section

$$\sigma_{jk} = \frac{A_{jk} N_j}{N_o (\frac{I}{e})} \equiv \frac{J_{jk}}{N_o (\frac{I}{e})} \tag{4.6}$$

where J_{jk} is the number of photons per cm per sec corresponding to the transition $j \rightarrow k$ in all directions along one cm of the beam path. The measurement of photon emission allows the determination of an emission cross section σ_{jk}. The level excitation cross section σ_j may be determined only if additional information on cascade terms and transition probabilities is available.

All the present measurements are carried out under the circumstances where the emission is linearly dependent on both the electron beam intensity and target gas pressure (see Figure 7). This ensures that no significant population of the excited states takes place through secondary mechanisms.

The optical detection system (see Figure 5) is a narrow band interference filter photometer which accepts radiation of wave length λ corresponding to the transition $j \rightarrow k$ emitted within a solid angle Ω_1 from a small section of the electron beam path ℓ, producing output

signal S_{jk}. If the radiation is assumed to be isotropic then the emission cross section can be computed from the following relation:

$$\sigma_{jk}\ (cm^2) = \frac{4\pi}{\Omega_1} \quad \frac{S_{jk}}{(I/e)\cdot \ell \cdot T_{eff}\ N_o\ S_\lambda} \quad , \qquad (4.7)$$

where $S_{jk} = \frac{N_s}{E_\lambda}$; N_s are the signal counts per second and E_λ is energy of the photons in ergs; T_{eff} is the filter factor (effective transmission coefficient of the interference filter) and S_λ is the quantum detection efficiency of the whole optical system. The value of S_λ is determined by substituting a tungsten filament lamp of known emissive power for the experimental source of emission and observing the output signal at the wave length of interest. (See details of calibration in section 4.5). The numerical value of S_λ is taken in terms of number of counts per erg.

The gas number density is given by

$$N_o = 2.687 \times 10^{19} \times \frac{273}{T} \times \frac{p}{760} \text{ molecules/cm}^3 \ ,$$

where p is the target gas pressure in mm of Hg and T is the gas temperature in K°.

The polarization of the emitted light can result in anisotropy of the radiation and hence an error in the determination of the emission cross section. A brief investigation of the polarization was made (see polarization section 4.4) using a simple polaroid analyzer which indicated that the error introduced in the cross section determination is negligible.

In all the measurements Ω_1 and ℓ were kept constant. Their values are 5.31×10^{-2} and 1.15 cm, respectively. The target gas

pressure is measured by an ionization gauge which is then calibrated against a high vacuum McLeod gauge (details are given in gauge calibration section 4.6).

4.2 Synthetic Spectra

The permitted transitions of N_2 and N_2^+ are shown in the energy level diagram given in Figure 8. The transition $B\ ^2\Sigma_u^+ \rightarrow X\ ^2\Sigma_g^+$ gives rise to the N_2^+ first negative system and the transition $A\ ^2\Pi_u \rightarrow X\ ^2\Sigma_g^+$ yields the N_2^+ Meinel system. The synthetic spectra of these two systems are discussed below.

4.2.1 N_2^+ ($B\ ^2\Sigma_u^+ - X\ ^2\Sigma_g^+$) First Negative System

(a) Wave Lengths

The $^2\Sigma$ states are described strictly by Hund's case (b) and therefore the selection rule $\Delta K = \pm 1$ holds, while $\Delta K = 0$ is forbidden. Generally the separation between the two sub-levels with $J = K + \frac{1}{2}$ and $J = K - \frac{1}{2}$ for a given K is very small compared to the separation of successive rotational levels. Each band consists of two branches, viz, a P branch and an R branch.

The wave numbers of the spectral lines corresponding to the transition between the two electronic states are given by (Herzberg, 1950 a):

$$\nu = \nu_e + \nu_v + \nu_r \quad , \tag{4.8}$$

where $\nu_e = T_e' - T_e''$, (4.9)

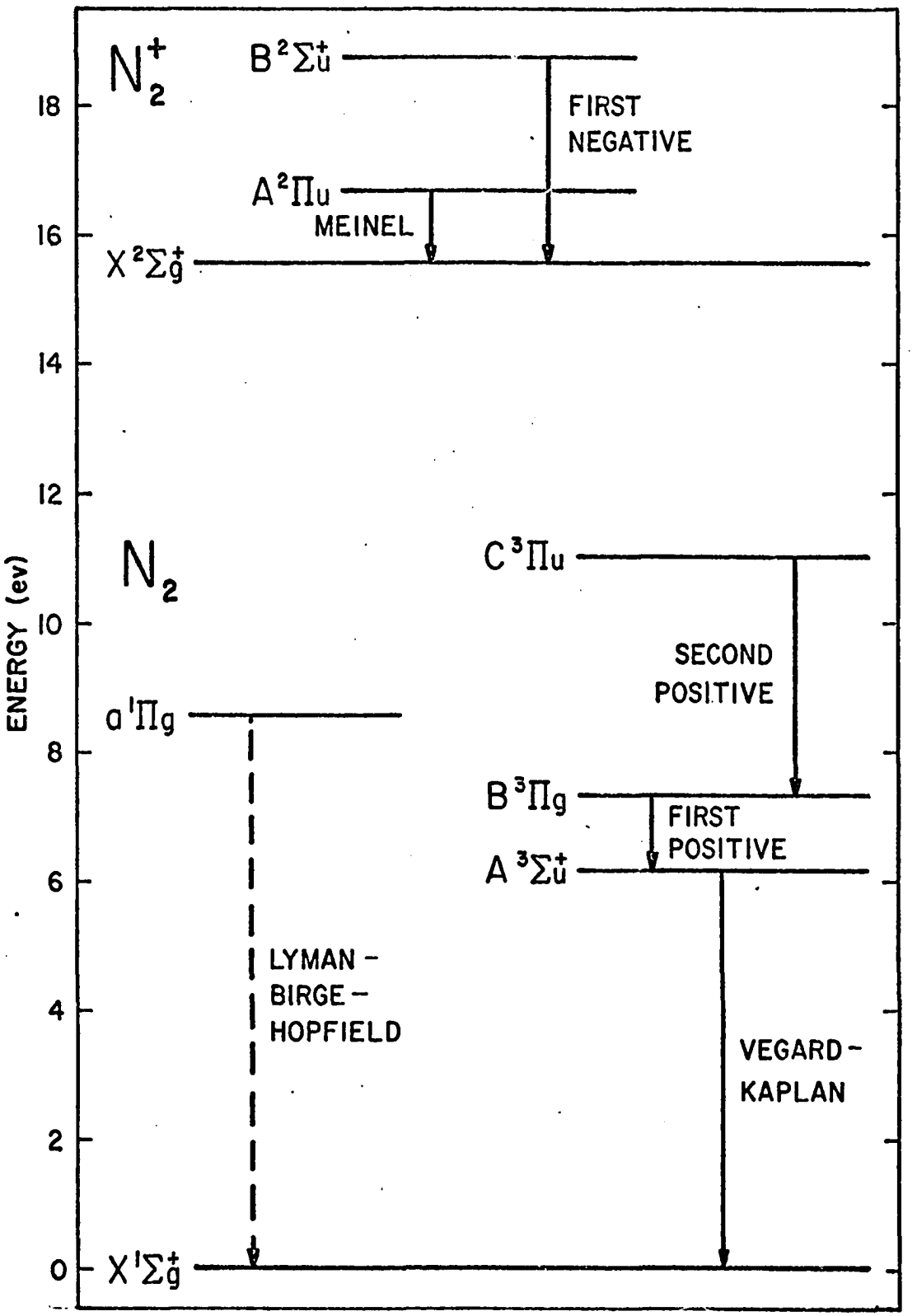

Figure 8 Partial energy level diagram of the N_2 molecule.

$$\nu_v = \omega_e' (v + \tfrac{1}{2}) - \omega_e' x_e' (v' + \tfrac{1}{2})^2 + \omega_e' y_e' (v' + \tfrac{1}{2})^3 - \omega_e'' (v'' + \tfrac{1}{2})$$

$$+ \omega_e'' x_e'' (v'' + \tfrac{1}{2})^2 - \omega_e'' y_e'' (v'' + \tfrac{1}{2})^3 \quad , \qquad (4.10)$$

and $$\nu_r = B_v' K' (K' + 1) - D_v' K'^2 (K' + 1)^2$$

$$- B_v'' K'' (K'' + 1) + D_v'' K''^2 (K'' + 1)^2 \quad . \qquad (4.11)$$

In equation 4.7,

$$B_v = B_e - \alpha_e (v + \tfrac{1}{2}) \quad ,$$

$$D_v = D_e + \beta_e (v + \tfrac{1}{2}) \quad ,$$

$$D_e = \frac{4B_e^3}{\omega_e^2} \quad ,$$

and

$$\beta_e = D_e \left[\frac{8\omega_e x_e}{\omega_e} - \frac{5\alpha_e}{B_e} - \frac{\alpha_e^2 \omega_e}{24 B_e^3} \right] \quad .$$

The various constants for the upper and lower states of the N_2^+ first negative system are given in the Table 2. These values are taken from Herzberg (1950b).

Table 2

Molecular Constants for B $^2\Sigma_u^+$ and X $^2\Sigma_g^+$ States of N_2^+ Molecule (cm^{-1})

State	T_e	ω_e	$\omega_e x_e$	$\omega_e y_e$	B_e	α_e
Upper B $^2\Sigma_u^+$	25461.5	2419.84	23.19	-0.5375	2.083	0.0195
Lower X $^2\Sigma_g^+$	0.0	2207.19	16.136	-0.0400	1.932	0.0200

The selection rule K" = K' + 1 gives a P branch while K" = K' - 1 gives an R branch.

(b) Intensity

The expression for the intensities in photons of the lines of a rotation-vibration band in emission is given by Herzberg (1950c),

$$I_{em} = I_A \frac{C_{em}}{Q_r} \nu^3 (K' + K'' + 1) e^{-B'_v K'(K' + 1)\frac{hc}{kT}} \qquad (4.12)$$

where I_A is an intensity alternation factor which is 2 for odd K' and 1 for even K' values and can be represented by the formula

$$I_A = 1.5 - 0.5 (-1)^{K'} \quad . \qquad (4.13)$$

The value for $B'_v = 2.010$ (Herzberg, 1950d) is taken for the ground state of N_2, assuming that the system is excited from the ground state of the N_2 molecule and the angular momentum of the molecule does not change during the excitation (i.e. $\Delta K = 0$). However, this assumption for the N_2^+ first negative is not critical, since the ground states of N_2 and N_2^+ ($B\ ^2\Sigma_u^+$) have similar rotational constants (Chamberlain, 1961b). The rotational temperature T is taken as 300°K, i.e., equal to the gas temperature. (Measurements of Polyakova et al. (1967) and Culp and Stair Jr. (1967) clearly indicate that the rotational temperature of the N_2^+ first negative band, excited by electron bombardment above 100 eV, is equal to the gas temperature.)

The relative intensity for the P branch is

$$I_p = [1.5 - 0.5 (-1)^{K'}] \nu_p^3 (K' + 1) e^{-B'_v K' (K' + 1) \frac{hc}{kT}} \qquad (4.14)$$

and for the R branch is

$$I_R = [1.5 - 0.5\ (-1)^{K'}]\ \nu_R^3\ (K')\ e^{-B'_v\ K'(K'+1)\ \frac{hc}{kT}} \qquad (4.15)$$

From the equations 4.8 - 4.15 the synthetic spectra for (0,0), (0,1) and (0,2) bands of N_2^+ first negative are computed

4.2.2 N_2^+ ($A\ ^2\Pi_u - X\ ^2\Sigma_g^+$) Meinel System

(a) Wave Lengths

The $^2\Sigma$ state always belongs to Hund's case (b) whereas, a $^2\Pi$ state may belong either to case (a) or to case (b) or to cases intermediate between (a) and (b).

If the $^2\Pi$ state belongs to Hund's case (b), and if the doublet separation in both the states ($^2\Pi$ - $^2\Sigma$) is so small that the doublet components cannot be separated in the spectrum, then there will be three branches P, Q and R, the Q branch being the most intense.

If the $^2\Pi$ state belongs to Hund's case (a), i.e., there is a large separation between $^2\Pi_{\frac{1}{2}}$ and $^2\Pi_{3/2}$, each of the bands of a ($^2\Pi$ - $^2\Sigma$) transition can be divided into two sub-bands, viz., ($^2\Pi_{\frac{1}{2}}$ - $^2\Sigma$) and ($^2\Pi_{3/2}$ - $^2\Sigma$), which are separated from each other by the amount of the doublet splitting of the $^2\Pi$ state. For each sub-band six branches are possible, making twelve branches in all (Herzberg, 1950e). There are eight main branches and four satellite branches. The intensity of the satellite branches is very small and decreases very rapidly with increasing K (Douglas, 1953).

In actuality, the $^2\Pi$ state belongs neither strictly to case (a) nor strictly to case (b), but represents a transition case which for

small rotations approximates to case (a) and for large rotations to case (b). Hence the formulas for a transition situation [i.e., from case (a) to case (b)] are used.

The expressions for ν_e and ν_v are the same which have been used for the first negative system (i.e., equations 4.8 and 4.9) and ν_r is given by (Herzberg, 1950f)

$$\nu_r = F(J') - F(K'')$$

where $F(K'') = B_v'' K'' (K'' + 1) - D_v'' K''^2 (K'' + 1)^2$.

For $J' = K' + \frac{1}{2}$; $F(J') = F_1(J')$ and

$$F_1(J') = B_v' [(J' + \tfrac{1}{2})^2 - 1 - \tfrac{1}{2} \{4(J' + \tfrac{1}{2})^2 + \lambda_v'(\lambda_v' - 4)\}^{\frac{1}{2}}] - D_v' J'^4 .$$

For $J' = K' - \frac{1}{2}$; $F(J') = F_2(J')$ and

$$F_2(J') = B_v' [(J' + \tfrac{1}{2})^2 - 1 + \tfrac{1}{2} \{4(J' + \tfrac{1}{2})^2 + \lambda_v'(\lambda_v' - 4)\}^{\frac{1}{2}}] - D_v'(J' + 1)^4 \qquad (4.10)$$

where $\lambda_v' = A/B_v'$. The other parameters have been defined in the previous section for the N_2^+ first negative bands.

The molecular constants of $A\ ^2\Pi_u$ state are taken from the work of Douglas (1953). However, some of the values listed in Douglas' paper are in error as pointed out by Mathews and Wallace (1961). The correct values used here are listed in Table 3.

Table 3

Molecular Constants of A $^2\Pi_u$ State of N_2^+ (cm^{-1})

$B_2 = 1.695$	$A_2 = -74.62$	$B_e = 1.740$
$B_3 = 1.678$	$A_3 = -74.60$	$\alpha_e = 0.018$
$B_4 = 1.658$	$A_4 = -74.58$	$D_e = 4 \times 10^{-6}$
$T_e = 9168.40$	$\omega_e = 1902.84$	$\omega_e x_e = 14.91$

The various branches with their appropriate selection rules are tabulated in Table 4.

Table 4

Branches of Meinel Bands

Sub-band	ΔJ	ΔK	Branches		Relationships
			Main ΔJ=ΔK	Satellite ΔJ≠ΔK	
F_1 (J'=K'+1/2)	-1	-2	-	$^{O}P_{12}$	J' = K' - 3/2
		-1	P_1	-	J' = K" - 1/2
	0	0	Q_1	-	J' = K" + 1/2
		-1	-	$^{P}Q_{12}$	J' = K" - 1/2
	+1	+1	R_1	-	J' = K" + 3/2
		0	-	$^{Q}R_{12}$	J' = K" + 1/2
F_2 (J'=K'-1/2)	-1	-1	P_2	-	J' = K" - 3/2
		0	-	$^{O}P_{21}$	J' = K" - 1/2
	0	0	Q_2	-	J' = K" - 1/2
		+1	-	$^{R}Q_{21}$	J' = K" + 1/2
	+1	+1	R_2	-	J' = K" + 1/2
		+2	-	$S_{P_{21}}$	J' = K" + 3/2

The wave lengths of the branches with the same ΔK values are very close to each other and cannot be separated in actual measurements. Thus in practice there is a total of eight branches, viz., $(P_1 + {}^{P}Q_{12})$, $(Q + {}^{Q}R_{12})$ P_1, ${}^{O}P_{12}$, P_2, $(Q_2 + {}^{Q}P_{21})$, $(R_2 + {}^{R}Q_{21})$ and ${}^{S}P_{21}$.

(b) Intensity

The relative intensities in photons are given by

$$I_i = \text{Const. } F_i \quad \nu^3 \quad i\,(J', \lambda_{v'})\, e^{-B_o K'(K'+1)\frac{hc}{kT}} ,$$

where F_i is an intensity alternation factor which is 2 for even K" and 1 for odd K", ν is the frequency of the "line", $i\,(J', \lambda_{v'})$ are the line strength factors given by Earls (1935) for the $^2\Pi - {}^2\Sigma$ transition. The exponential term is the Boltzmann factor for the ground state of N_2 $(X\ {}^1\Sigma_g^+)$ for $v = 0$. [It is assumed that the excitation takes place from the ground state of N_2 and there is no change of angular momentum, i.e., $\Delta K = 0$ (see Chamberlain, 1961b)]. The rotational temperature T is taken equal to the gas temperature, i.e., $300^{o}K$.

The line strength factors given by Earls (1935) are the following:

$$i\,(P_2, {}^{O}P_{12}) = \frac{(2J+1)^2 \pm (2J+1)\,U\,(4J^2+4J+1-2\lambda)}{32\,(J+1)} ,$$

$$i\,({}^{Q}P_{21}, P_1) = \frac{(2J+1)^2 \mp (2J+1)\,U\,(4J^2+4J-7+2\lambda)}{32\,(J+1)} ,$$

$$i\,(Q_2, {}^{P}Q_{12}) = \frac{(2J+1)\,[(4J^2+4J-1) \pm U\,(8J^3+12J^2-2J+1-2\lambda)]}{32J\,(J+1)} ,$$

$$i\,({}^{R}Q_{21}, O_1) = \frac{(2J+1)[(4J^2+4J-1) \mp U\,(8J^3+12J^2-2J-7+2\lambda)]}{32J\,(J+1)} \quad ,$$

$$i\,(R_2, {}^{Q}R_{12}) = \frac{(2J+1)^2 \pm (2J+1)\,U\,(4J^2+4J-7+2\lambda)}{32J} \quad ,$$

$$i\,({}^{S}P_{21}, P_1) = \frac{(2J+1)^2 \mp (2J+1)\,U\,(4J^2+4J+1-2\lambda)}{32J} \quad ,$$

where $$\lambda = \frac{A_v}{B_v} \quad ,$$

$$U = [\lambda^2 - 4\lambda + (2J+1)^2]^{-\frac{1}{2}}$$

and for U a positive root value is taken. For a special case of $J' = \frac{1}{2}$ with $\lambda < 0$;

$$i\,(P_2) = i\,({}^{Q}P_{21}) = 1/6 \quad ,$$

$$i\,(Q_2) = i\,({}^{R}Q_{21}) = 1/3 \text{ and}$$

for all other branches, it is identically zero.

Using the above formulas, the frequencies and relative intensities for various lines of different branches of the (2,0), (3,1) and (4,1) N_2^+ Meinel bands were computed on an IBM 360 computer.

4.3 Filter Transmission

All the six filters used are 2" circular Fabry-Perot type interference filters having a narrow band-pass, manufactured by Thin Film Products, Inc., Cambridge, Massachusetts. The transmission peaks of these filters are near the wave lengths studied and are nearly opaque in the other spectral regions of S-20 and S-1 photocathode surfaces.

The transmission curves for each filter were supplied by the manufacturer and were also recorded in the laboratory using a half meter Jarrell - Ash double beam scanning spectrophotometer. The characteristics of all the filters used are shown in Table 5.

Table 5

Filter Characteristics

Filter Number	Band	Peak		Half Width (A^{o})
		Wave Length (A^{o})	Transmission (%)	
1	(0,0) N_2^+ 1NG	3902	26.0	36
2	(0,1) N_2^+ 1NG	4282	44.5	52
3	(0,2) N_2^+ 1 NG	4706	80.0	33
4	(4,1) N_2^+ M	7065	73.4	55
5	(2,0) N_2^+ M	7848	72.5	50
6	(3,1) N_2^+ M	8085	66.0	50

The filter transmission factors are calculated by the following formula

$$F = \frac{\sum_{B} (\text{Intensity of each line}) \times (\text{Transmission of the filter at that wave length})}{\sum_{B} \text{Intensity of each line}},$$

where $\sum_{B}$ is the total sum of the intensity of all the branches.

The intensities of the bands have been integrated from K' = 0 to K' = 30 since, the "lines" with K' > 30 have a little (or no) contribution in the total band intensity. Contributions of other bands, if any, present within the transmitting regions of the filters, have been estimated and corrections are applied in the final results.

4.4. Polarization

J. A. Smit (1935) has given an expression for the intensity of radiation observed at some angle, θ, relative to the projectile axis in terms of the total emitted intensity and the polarization of the radiation (assuming cylindrical symmetry about the projectile axis),

$$I(\theta) = \frac{3I_o}{4\pi} \left[\frac{1 - P\,\mathrm{Cos}^2\theta}{3 - P}\right],$$

where I_o is the total emitted radiation intensity.

If the observations are made at $\theta=\theta_o = 54^o\ 44'$, the above expression would reduce to

$$I(\theta_o) = \frac{I_o}{4\pi},$$

and the dependence of the radiation on P vanishes. However, in this experiment, the radiation is observed at $\theta = 90^o$ and it is necessary to check the polarization of the emitted light.

The usual formula for the polarization is

$$P = \left.\frac{I_{\parallel} - I_{\perp}}{I_{\parallel} + I_{\perp}}\right|_{90^o}$$

where $I_{||}$ and $I_{\perp}$ are radiation intensities at 90° to the incident projectile axis with electric vectors parallel and perpendicular, respectively, to the plane defined by the incident projectile beam axis and the propagation vector of the resulting photon.

A circular polaroid analyzer is inserted between the quartz window and the collimator aperture. The axis of the analyzer is kept parallel to the beam direction and the output of the photometer ($I_{||}$) is recorded. Again, the axis is made perpendicular to the beam direction and $I_{\perp}$ is recorded. It may be mentioned that the aim of this experiment is not to measure an absolute value of polarization or to find its dependence on energy but to estimate the amount of polarization present. Several sets of readings were taken and it was found that the polarization decreases rapidly with increasing electron beam energy.

The amount of polarization is less than 2% for N_2^+ first negative bands and 2.5% for all the N_2^+ Meinel bands at 100 ev electron energy.

4.5 Calibration of Photometers

Both the photometers are calibrated against two standard ribbon type tungsten lamps U-94 and E-82 supplied by the National Bureau of Standards and are used according to the instructions described in "Standard of Spectral Radiance for the Region of 0.25 to 2.6 Microns" by Stair et al. (1960). These lamps have fused silicon window and are operated at about 6 volts drawing a current of 25 to 35 amperes from a specially designed power supply [Stair et al. (1960)] which gives a

constant current during the operation. The lamp U-94 operating at 35 amperes has been calibrated in the radiating region from 2500 Å to 7500 Å and is used for calibrating the N_2^+ first negative and (4, 1) Meinel bands photometers. The calibration of the lamp E-82, operating at 25 and 30 amperes is from 0.5μ to 2.6μ and is used to calibrate the N_2^+ Meinel bands photometers. The λ 7059 (4,1) N_2^+ Meinel band photometer was calibrated against both the lamps (since the calibration for both the lamps is available in this region). The value obtained for S_λ, in both of the cases, was within one percent. This gives an added confidence in the absolute value of the emissivity of these lamps and also in the method used for calibration. The energy output of these lamps are given in a tabular form in units of micro watts per steradian - millimicron - mm^2 of source. A "smooth curve" is drawn from the given data points. The spectral radiance at a particular wave length is then read directly from the "smooth curve".

A diagram of the calibration system is shown in Figure 9. M_1 is a spherical mirror with a radius of curvature of one meter and is placed at a distance of one meter from the filament of the lamp. The plane mirror M_2 is set at about 60 cm from the spherical mirror facing it at an angle of less than 10^o. The light from the standard lamp fully illuminates the spherical mirror and is contained within a cone of 5^o. All angles of reflection are kept within 10^o. The image (unit magnification) of the standard lamp filament is focussed at a circular aperture S having an area of 1.17 mm^2 and the central part of the filament is observed through it. The collimator assembly including the

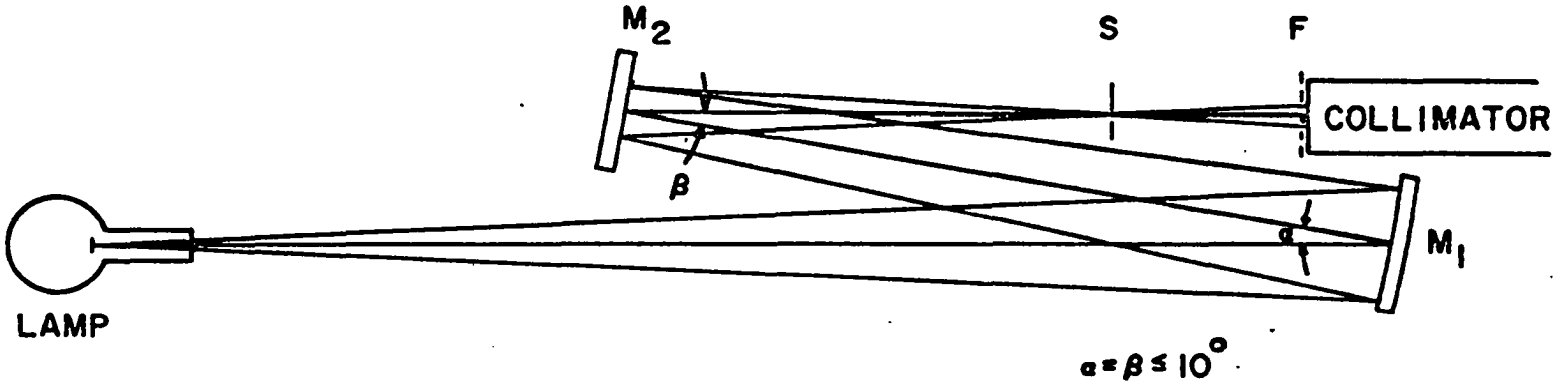

Figure 9 Calibration of photometers.

quartz window is placed at a distance from the aperture, S, equal to the distance between the electron beam and the quartz window, such that the image of the filament replaces the electron beam path and the actual conditions of the experiment are reproduced (see collimator section 2.7).

Extra Kodak filters whose transmission factors are determined in the laboratory are placed before the quartz window to avoid excessive current in the photometer. The light from S passes unobstructed through the aperture and the slit (inside the collimator assembly).

The solid angle subtended by the photometer is determined by the diameter of the spherical mirror which is fully illuminated by the light from the standard lamp, and its distance from the filament.

The possibility of polarization in the standard lamp radiation due to reflection at two mirrors is checked, revealing no polarization. The same areas of the photocathode are used during the calibration and the measurements. The spectral response of the standard lamps and the reflectivity of the aluminized mirrors have been supplied by the National Bureau of Standards.

4.6 Calibration of Ionization Gauges

During the experiment the collision chamber pressure is measured by a Veeco RG-75K ionization gauge which is calibrated against a CVC high vacuum McLeod gauge Model No. GM-110. The volume of the McLeod gauge is 2193 cc, capillary diameters are 0.535 mm and the gauge requires 75 lbs. of mercury.

The McLeod gauge (Figure 10) is basically a compression device used to extend the range of the manometer. The McLeod gauge equation as derived from Boyle's law is as follows: (cf. Carr 1964)

$$PV = (sH)\ \Delta h \quad , \tag{4.16}$$

or

$$P = K\ H\ \Delta h \quad , \tag{4.17}$$

where $K = s/V$.

P is the pressure (Torr) in the gauge before compression, V is the volume (cc) of the bulb plus the closed end capillary, s is the cross sectional area (cm^2) of the closed capillary, H is the distance (cm) from the top of the closed capillary to the top of the mercury level in the capillary and Δh is the final pressure measurement in mm of Hg.

The gauge is calibrated by the measurement of its dimensions, s and V. The compression of gas by mercury must be slow enough so that the final temperature of the compressed gas is the same as the uncompressed gas.

4.6.1 Sources of Error

The chief sources of systematic errors present in the McLeod gauge are reviewed by Carr (1964) and are the following:

(1) Deviations from Boyle's law;

(2) The different capillary depression in the capillaries;

(3) The presence of the cold trap used to isolate the mercury vapors in the McLeod gauge from the rest of the system.

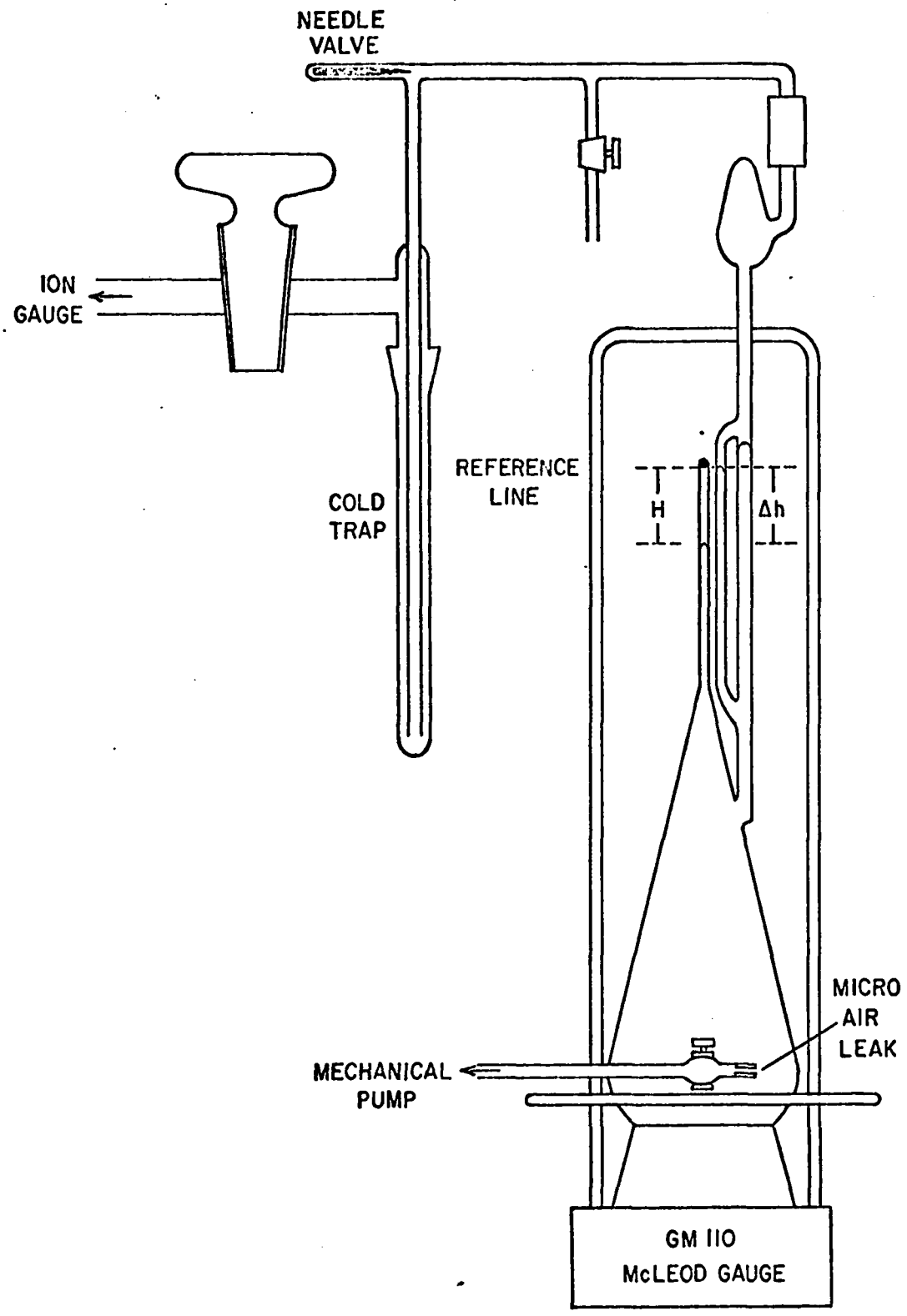

Figure 10 Modified McLeod gauge assembly for the calibration of ionization gauge.

Any of these can cause an error of at least 10 percent and are discussed below in turn.

Deviation from Boyle's law includes (i) the effect of gases which condense during compression, (ii) the fact that a real gas obeys a non-ideal gas law such as that expressed by the van der Waal equation and (iii) absorption and desorption on the walls of the gauge. Since N_2 is a permanent and non-condensible gas over the pressure range encountered in a McLeod gauge, (i) is not of any importance. However, the presence of residual gases such as water vapors and carbon dioxide can introduce errors. This is avoided by baking the gauge above 400°C while it is under high vacuum. The van der Waal equation which accounts for the finite size of the gas molecules and the forces between them causes at the most only a 0.5 percent deviation from the perfect gas law (Jansen et al. 1959) the most important deviation from the perfect gas law being the effect of absorption and desorption on the walls of the system. A bake out at 400°C is very effective in removing molecules loosely bound to the walls by van der Waal's forces, and also minimizes the sorption error.

The second source of error is caused by the surface force between the mercury and the glass. The smaller the diameter of the capillary, the greater is the depression of the surface of mercury. Capillary depression is also a function of temperature, cleanliness of the mercury-glass surface interface, roughness of the surface and the impurities in the mercury, etc. The depression of the mercury in the two tubes is in general different even when they have identical

cross sections and the whole system is clean.

One must then add the term $\Delta h_d(H)$, the difference in capillary depression, between the two capillaries (which is generally a function of H) and the absorption coefficient 'a' to the McLeod gauge equation 4.17 ('a' has the dimensions of length) (see detailed derivation in Carr, 1964).

$$P = K' [\Delta h + \Delta h_d (H)] (H + a) \quad ,$$

where

$$K' = \frac{s}{V[1+3a(\frac{4\pi}{3V})^{1/3}]} \quad . \qquad (4.18)$$

Kreisman (1960) has performed a series of experiments with bakeable McLeod gauges in an ultra high vacuum system which show that with careful techniques the sorption error can be made negligible and that a correction can be made for the capillary depression error.

The third systematic error arises in the cold trap used to isolate the McLeod gauge mercury, which has a vapor pressure of 10^{-3} Torr at room temperature, from the gauge being calibrated. The mercury streaming from the McLeod gauge into the trap sweeps along other gas molecules and exerts the same pumping action occurring in a diffusion pump.

4.6.2 Elimination of Errors

As discussed earlier, the sorption errors can be made negligible by a careful heating and degassing of the McLeod gauge while it is under high vacuum.

The capillary depression correction Δh_d is obtained by a series of variable compression measurements. The mercury is raised slowly and after it has filled the volume V, a reading of H and Δh is made as the mercury rises to successively higher levels in the capillaries, thus giving a series of readings for the same initial pressure P. If 'a' is negligible compared to H then equation 4.18 can be written as

$$\Delta h + \Delta h_d = \frac{P}{K'} \frac{1}{H} \quad . \tag{4.19}$$

Thus a plot of Δh versus $1/H$ would give a straight line of slope P/K' which intercepts the Δh axis at $-\Delta h_d$. Figure 11 represents a series of such straight lines made for a particular gauge with different pressures. The data points on a straight line also indicate that 'a', the sorption coefficient, is negligible.

Another method, depending upon the variable depression technique [cf. Podgurski and Davis (1960)] is used. In this method the open capillary in a conventional McLeod gauge is ignored, and the side arm is used to record the Δh (see Figure 10), since the variation of the capillary depression in a wide tube are negligible. A set of readings using this method are shown in Figure 12.

Meinke and Reich (1962) have made a theoretical calculation for the pressure difference between two systems due to the presence of a cold trap, and have verified them experimentally. The ratio γ of the pressure P_2 (in Torr) indicated by the gauge being calibrated to the pressure P_1 in McLeod gauge is given by

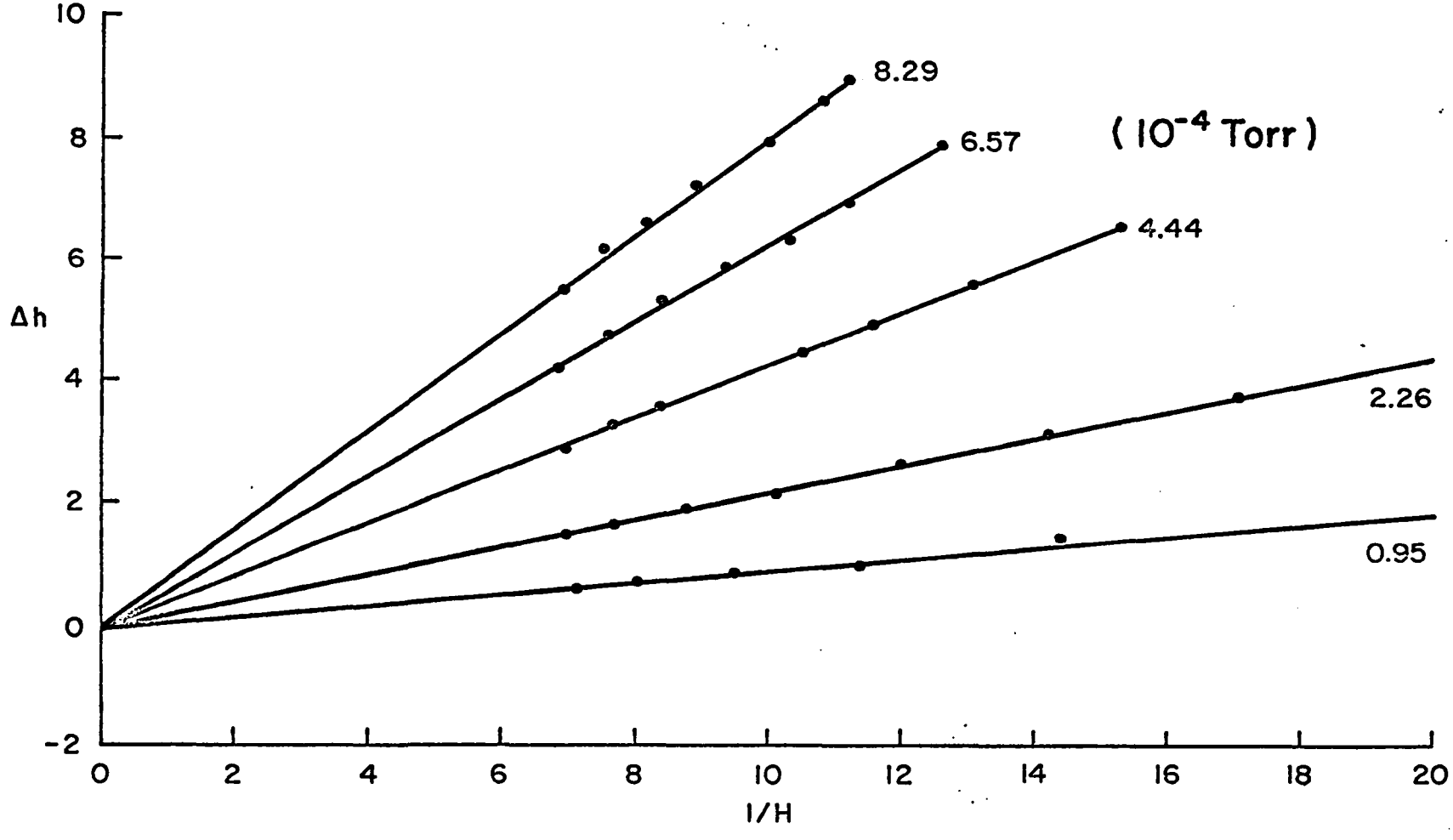

Figure 11 Pressure calibration by the variable compression technique, using the open end capillary.

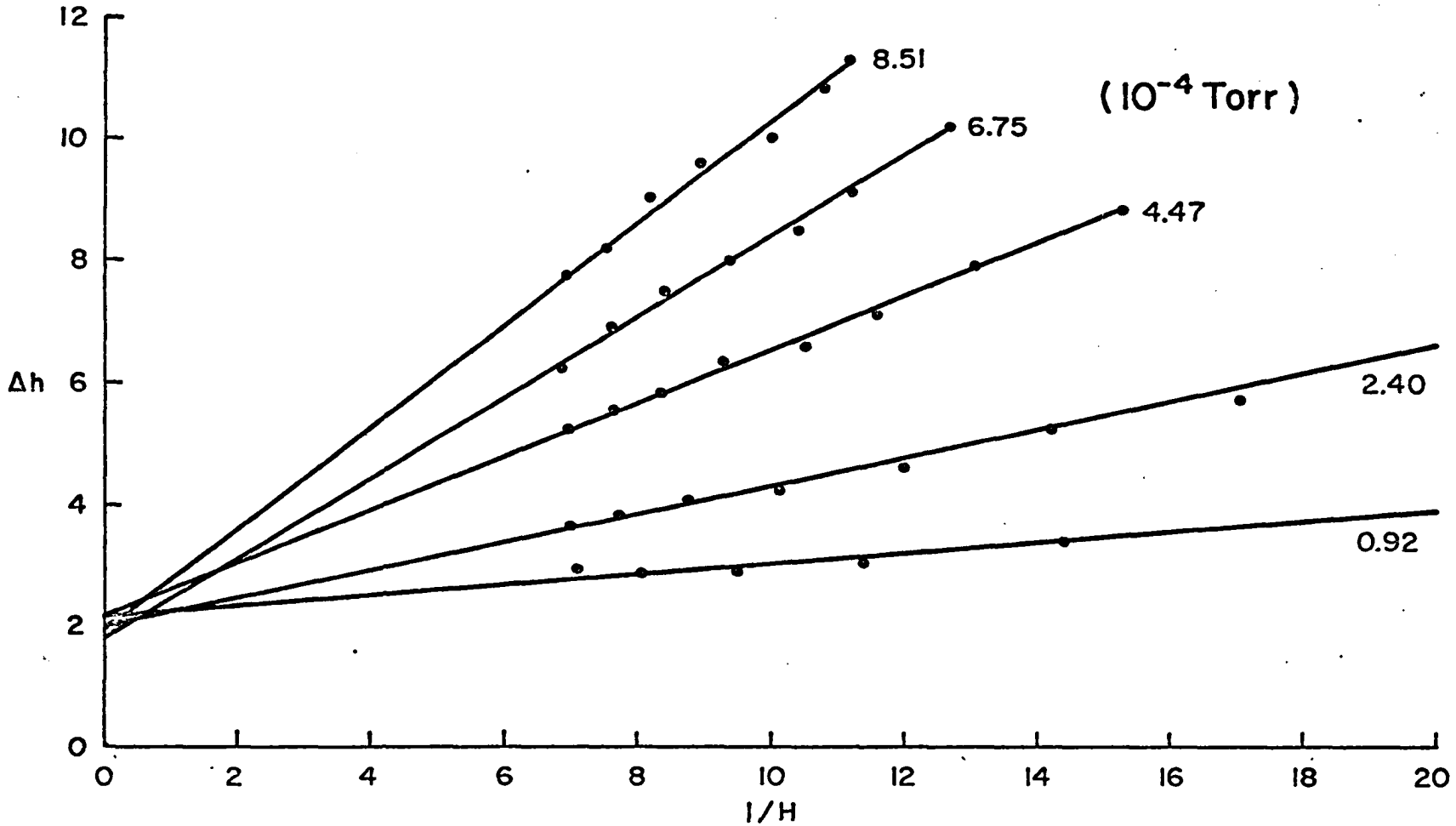

Figure 12 Pressure calibration by the variable compression technique, using the wide side arm.

$$\ln \gamma = \frac{P_d f}{1 + P_1 f} ,$$

$$\text{where} \quad f = 6.91 \times 10^{19} \cdot r \cdot \frac{(a_g + a_d)^2}{T\sqrt{1 + \frac{M_d}{M_g}}} ,$$

P_d is the vapor pressure of mercury in Torr, at room temperature, T is the room temperature, r is the radius of the tubulation from the McLeod gauge to the trap in cm, a_g and a_d are the effective radii (cm) of the gas and the mercury molecules respectively, from kinetic theory and M_g and M_d the respective molecular masses in grams mole^{-1}.

Cooling the mercury reservoir would reduce this error, but it is very cumbersome to cool the large quantity of mercury (about 75 lbs.). Moreover, a difference in temperature between the McLeod gauge and the gauge under calibration will introduce an error due to thermal transpiration effects. However, since γ is a function of r, γ can be decreased by decreasing r by means of a needle valve. A bakeable needle valve was put at the mouth of the cold trap as shown in Figure 10. When the sensitivity of the gauge under calibration does not change by a slight change of r, γ will be equal to one, to within the accuracy of the measurement.

The presence of cold trap alone can produce errors as large as 10 percent in some cases. Two volumes having the same temperature and with a cold trap between them can have an apparent pressure difference if the radius of the tube joining them is not uniform throughout. Rusch and Bunge (1932) found that the pressure difference is a sensitive function of the dimensions of the trap. By studying the

pressure difference as a function of the relative diameters of the cylindrical re-entrant type trap they arrived at the empirical relation that when the inside diameter of the inner tube is equal to the difference between inside diameter of the outer wall minus the outside diameter of the inner tube, the pressure difference could be made negligible. A special cylindrical re-entrant type trap is made to conform to this requirement.

Furthermore, the volume of the system is large and the raising of mercury in the McLeod gauge does not alter the pressure of the system.

Moreover, the mercury is raised from a point just below the cut-off of the bulb and adequate time is allowed for the pressure in the McLeod gauge bulb to come to an equilibrium with the gauge being calibrated. The rising of mercury is maintained at a very slow rate without violent bubbling to avoid building up of an electric charge which would affect the function of the gauge. The pressure calibrations were made by using dry ice as well as liquid N_2 in the cold trap. Strikingly, in both cases, after making a proper adjustment of the backable needle valve, the pressure calibrations were within 2%. This clearly indicates that the thermal transpiration effects were negligible.

The maximum estimated error in the pressure measurement is probably about 5% after taking all the necessary precautions as outlined above.

CHAPTER V

EXPERIMENTAL RESULTS AND DISCUSSION

In this chapter, the emission cross sections for the N_2^+ first negative [(0,0), (0,1) and (0,2)] bands and the N_2^+ Meinel [(4,1), (2,0) and (3,1)] bands produced by the electron impact are presented. Also, the measured cross sections are compared with available experimental and theoretical results.

5.1 N_2^+ First Negative Bands

The emission cross sections for the (0,0), (0,1) and (0,2) bands at various energies (from 70 eV to 4 keV) are shown in Figure 13 and tabulated in Table 6. The maximum values of the cross sections occur at about 90-100 eV and are marked by an asterisk (*). These data points represent an average of about ten independent readings at every energy. The maximum scatter of the data points was less than 5%, and the day-to-day reproduction was better than 5%. Results of McConkey and Latimer (1965) and those of Holland (1967) at 907 eV are also shown in Figure 13 as a comparison.

Corrections are made for the contribution of other bands lying in the band pass of the filters. The λ3914 (0,0) band is contaminated by the λ3884 (1,1) band of the N_2^+ first negative band. From the synthetic spectra of these bands and the transmission curve of the filter, the effective transmission of both bands through the filter was determined with a computer. Using these filter factors, Einstein A coefficients

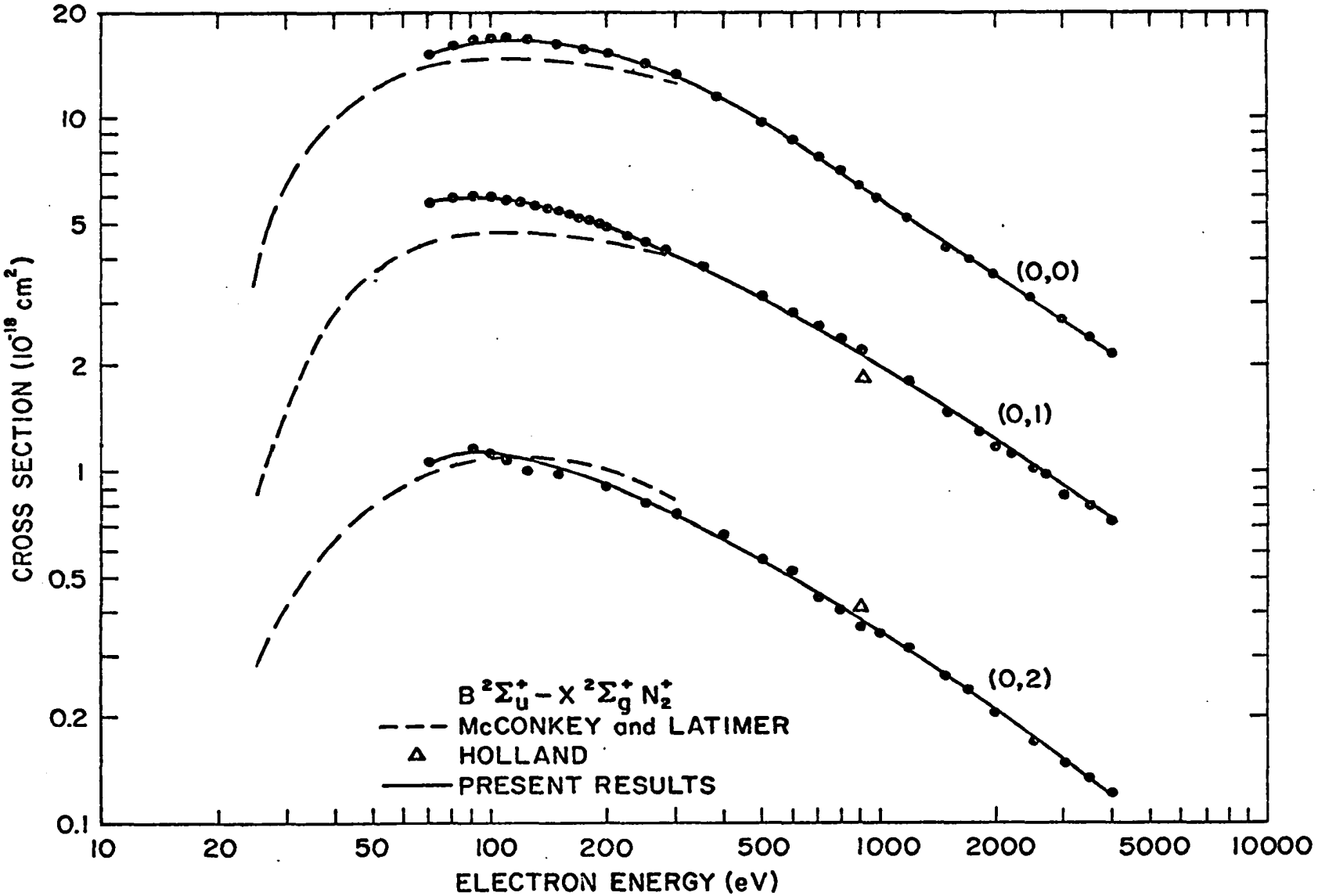

Figure 13 Emission cross sections for the N_2^+ first negative bands produced by electron impact.

TABLE 6

Emission Cross Sections of N_2^+ First Negative Bands (cm^2)

E	(0,0) (10^{-18})	(0,1) (10^{-18})	(0,2) (10^{-19})
70	15.05	5.76	10.77
90	16.54	6.06*	11.64*
100	16.86*	5.85	11.06
110	16.86	5.81	10.78
150	16.25	5.49	9.81
200	15.23	4.89	9.16
250	14.13	4.47	8.14
300	13.06	4.00	7.63
500	9.69	3.14	5.60
600	8.59	2.76	5.21
700	7.81	2.56	4.41
800	7.02	2.38	4.09
900	6.52	2.20	3.74
1500	4.50	1.49	2.69
2000	3.65	1.18	2.05
2500	3.10	1.02	1.70
3000	2.65	0.86	1.49
3500	2.40	0.80	1.33
4000	2.10	0.73	1.21

given by Nicholls (1963) and relative population of v_0 to v_1 levels as 9:1, measured by Sheridan and Clark (1965) for proton and electron impact and calculated by Franck-Condon factors (Nicholls, 1961), the ratio between the intensities of the (1,1) and (0,0) band observed through the filter was obtained. The contribution due to the (1,1) band was about 2% in the measurement of the (0,0) band cross section. The same correction factor was made over the whole energy range assuming that the relative band profile and intensity do not change with the energy (both bands are directly excited by the primary electrons, neglecting secondary effects, at low pressures of 10^{-4} Torr in the collision chamber). Even if there is a change in the relative band intensity with the energy of electrons, the error is negligible, since the total intensity of the (1,1) band is only a few percent of that of the (0,0) band [recent measurements of Havakawa et al. (1965) indicate that the absolute intensity of the (1,1) band is only 1% of the (0,0) band]. Similar considerations lead to a 3% contribution in the measurements of λ4278 (0,1) band due to (1,2) band of the N_2^+ first negative system.

The emission cross sections are uncorrected for the polarization which was less than 2% at 100 eV electron energy in all cases. Cross sections were measured at 500 eV - 1 keV electron energy with and without the radial magnetic field, which was used for the collimation of beam in the collision chamber. No variation in the output intensity (signal/beam current) was observed. Also, by varying the magnetic field

from 100-250 G, no variation in output intensity was observed, indicating that the magnetic field had no undesirable effects on the excitation.

5.1.1 Comparison with other results

The absolute emission cross sections of all three bands [(0,0), (0,1) and (0,2)] have been measured twice previously [McConkey and Latimer (1965); Stewart (1956)] and recently Nishimura (1968) has also measured them relative to (0,0) band. The results of McConkey and Latimer (1965) are in good agreement with the present results where they overlap (see Figure 13). The measurements of Holland (1967) at 907 eV are also in good agreement. However, the present cross sections are a factor of 2.5 higher than those of Stewart (1956) and Nishimura (1968) which have been omitted from Figure 13 for the sake of clarity.

Figure 14 shows all available measurements for the λ3914 (0,0) emission cross section and compares them with the present result. The measurements of Holland (1967) are in good agreement with the present result over the common energy range but are lower by 10 to 12 percent. The measurements of McConkey et al. (1967) are in excellent agreement above 300 eV. However, their cross sections are 4-12 percent lower in the low energy range. The differences between the present results and those of Holland (1967) and McConkey et al. (1967) are well within the quoted experimental accuracies. The values of Sheridan, Oldenberg and Carleton (1961), Stewart (1956) and Hayakawa and Nishimura (1964) are in poor agreement, and the present results are higher by a factor of 2 to 3.

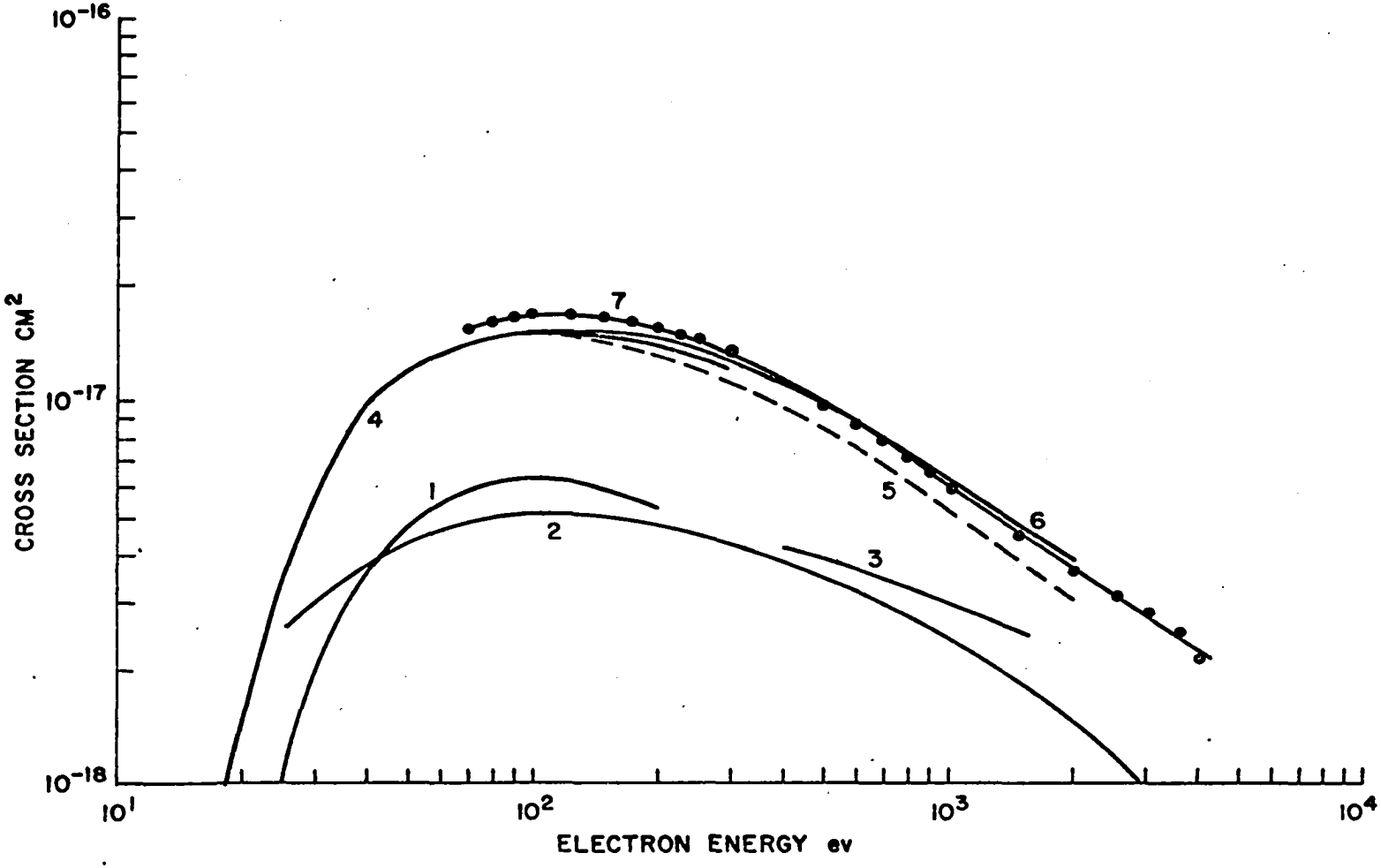

Figure 14 Comparison of the electron excitation cross sections of λ 3914: (1) Stewart (1956); (2) Sheridan, Oldenberg and Carleton (1961); (3) Hayakawa and Nishimura (1964); (4) McConkey and Latimer (1965); (5) Holland (1967) (6) McConkey, Woolsey and Burns (1967); (7) present results.

The cause of the disagreement with the results of Sheridan et al. (1961), Stewart (1956) and Hayakawa and Nishimura (1964) cannot be explained, owing to the absence of details of photometric and pressure calibration in their papers.

The relative transition probability of λ3914, λ4278 and λ4709 of v'=0 progression of N_2^+ first negative bands are compared with other theoretical and experimental values in Table 7.

5.1.2 Comparison with Total Ionization Cross Section of N_2

The emission cross sections of N_2^+ first negative bands are similar to the total ionization cross section of N_2 by electron impact. Dalgarno et al. (1965) have reported that the λ3914 emission cross section is nearly 6% of the total ionization cross section of N_2 above 100 eV. However, this value depends upon the choice of ionization cross section used in the calculation. In Table 8 the ratio of λ3914 cross section to the ionization cross sections of Tate and Smith (1932), Rapp and Englander-Golden (1965) and Schram et al. (1965, 1966) are shown. The mean ratio of the λ3914 cross section to the total ionization cross section comes out to be 0.068.

In Figure 15 the ratios of total ionization cross section of Rapp and Englander-Golden (1965) to the emission cross section of λ3914 have been plotted. In Figure 16 the excitation cross section of the v'=0 [sum of (0,0), (0,1) and (0,2)] vibrational level of the $B\ ^2\Sigma_u^+$ state of N_2^+ are compared with the total ionization cross section [Rapp and Englander-Golden (1965) and Schram et al. (1965), (1966)] of N_2 by

TABLE 7

Relative Transition Probabilities of the v'=0 Progression in the N_2^+ First Negative System

Investigators		λ3914 (0,0)	λ4278 (0,1)	λ4709 (0,2)	Method
Herzberg	(1928)	1.0	0.38	0.058	Measured in N_2 discharge
Pillow	(1951)	1.0	0.34	0.119	Calculated
Bates	(1952)	1.0	0.31	0.071	Calculated
Wallace and Nicholls	(1955)	1.0	0.33	0.074	Measured in N_2 negative glow
Stewart	(1956)	1.0	0.39	0.105	Electron impact excitation
Philpot and Hughes	(1964)	1.0	0.32	0.067	Proton impact excitation
Hayakawa et al.	(1965)	1.0	0.43	0.084	Electron impact excitation
McConkey and Latimer	(1965)	1.0	0.32	0.084	Electron impact excitation
Sheridan and Clark	(1965)	1.0	0.53	0.125	Ion impact excitation
Holland	(1967)	1.0	0.33	0.075	Electron impact excitation
Nishimura	(1968)	1.0	0.29	0.059	Electron impact excitation
Present Results		1.0	0.34	0.065	Electron impact excitation

TABLE 8.

Ratios of N_2 Total Ionization Cross Sections to λ3914 Excitation Cross Sections

Energy (ev)	Ratios		
	Tate and Smith (1932)	Schram et al. (1965) and (1966)	Rapp and Englander-Golden (1965)
70	17.81		15.48
90	17.35		15.04
100	17.19	14.59	14.96
110	17.12		14.99
150	17.04		15.10
200	16.68	13.79	14.91
250	16.55		14.75
300	16.36	13.17	14.68
500	16.15	13.11	14.97
600	15.96	13.39	15.05
700	15.76	13.06	14.87
800		13.19	15.16
900		12.94	15.11
2000		12.58	
2500		12.29	
3000		12.38	
3500		12.08	
4000		12.48	
Averages	16.72	13.00	15.01

Mean = 14.9

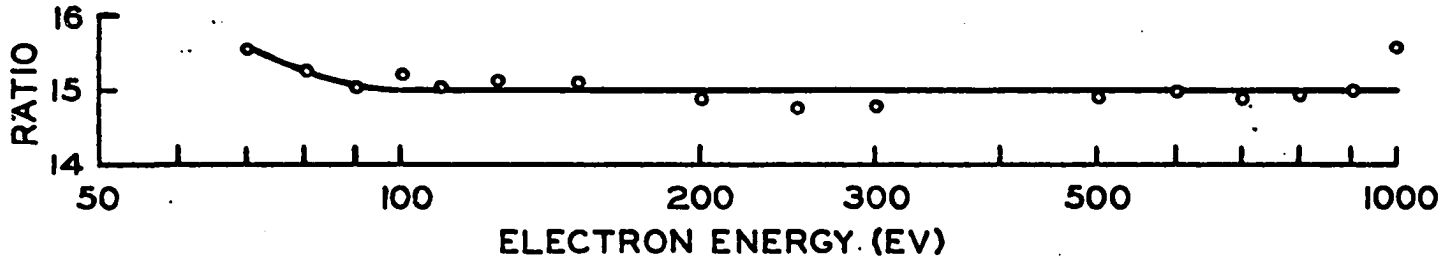

Figure 15 Ratio of the total ionization cross section of N_2 to the emission cross section of λ 3914 by electron impact.

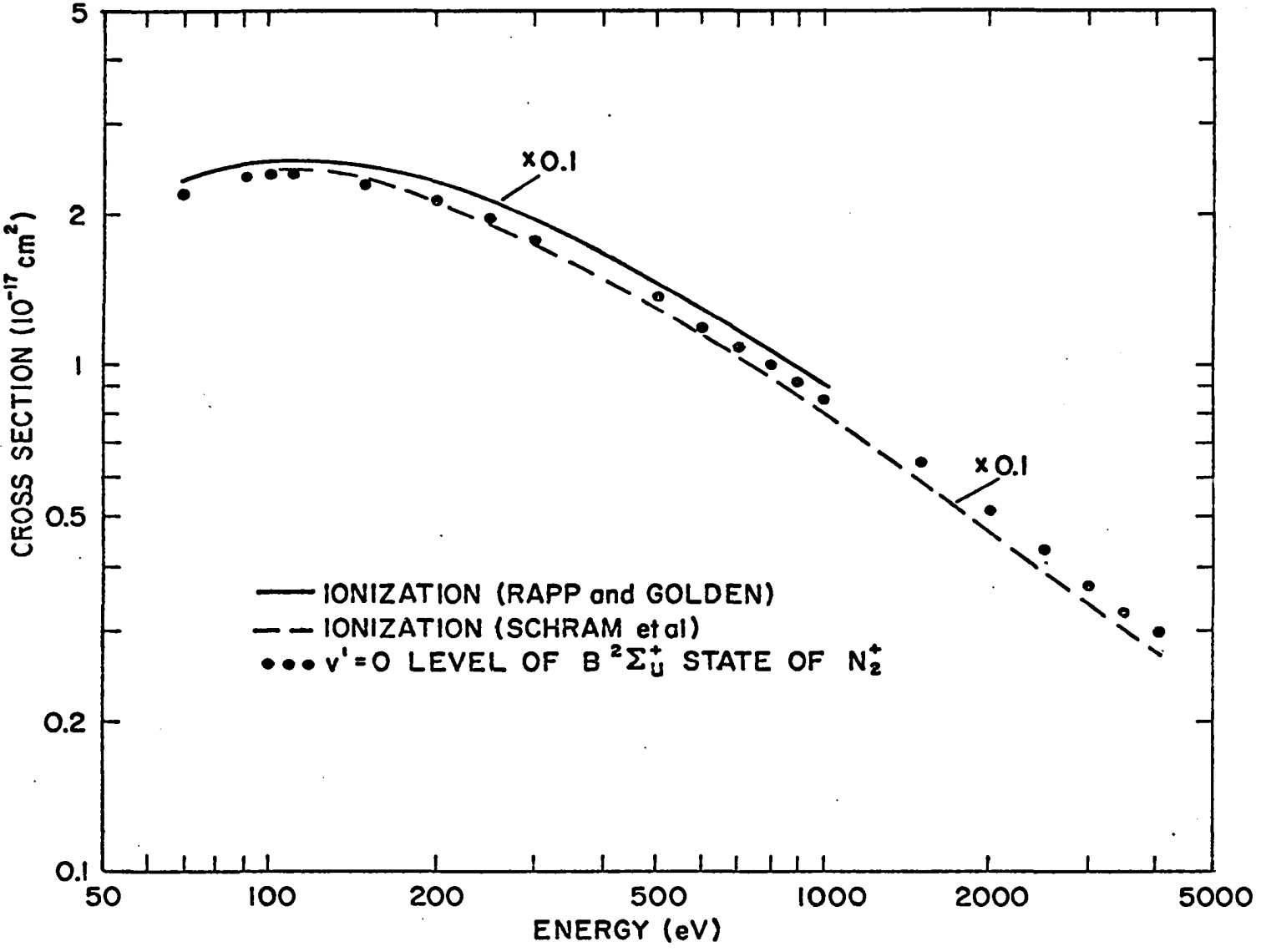

Figure 16 The total ionization cross section of N_2 and the emission cross section of v' = 0 vibrational level of B $^2\Sigma_u^+$ state of N_2^+ by electron impact.

electron impact. The v'=0 vibrational level accounts for 10% of the total ionization cross section. This result is in excellent agreement with that of Dahlberg et al.(1967) for proton bombardment at higher energies.

5.1.3 Comparison with Theory

The excitation of the N_2^+ first negative system is mainly by simultaneous ionization and excitation of N_2 molecules leaving N_2^+ ions in the $B\ ^2\Sigma_u^+$ excited state and is a constant fraction of the total ionization of N_2 [see Section 5.1.2]. This means the excitation cross section can be represented similar to the Bethe-Born approximation equation for ionization [cf. Schram et al. (1965)],

$$\sigma_e = \frac{4\pi a_o^2 R}{E_{el}} M_e^2 \ln C_1 E_{el} , \qquad (5.1)$$

where σ_e is the excitation cross section in cm^2, a_o is the first Bohr radius, R is the Rydberg energy, E_{el} is the electron energy corrected for relativistic effects, C_1 is a constant and M_e^2 is the effective dipole matrix element for excitation, squared.

From the above equation (5.1), it can be seen that a plot of $\frac{\sigma_e E_{el}}{4\pi a_o^2 R}$ versus $\ln E_{el}$ will allow one to determine the value of M_e^2. Such a plot is given in Figure 17 for the v'=0 vibrational level [sum of (0,0), (0,1) and (0,2) cross sections] of the $B\ ^2\Sigma_u^+$ state. The value of M_e^2 from the graph is 0.51. Also the measured cross sections very

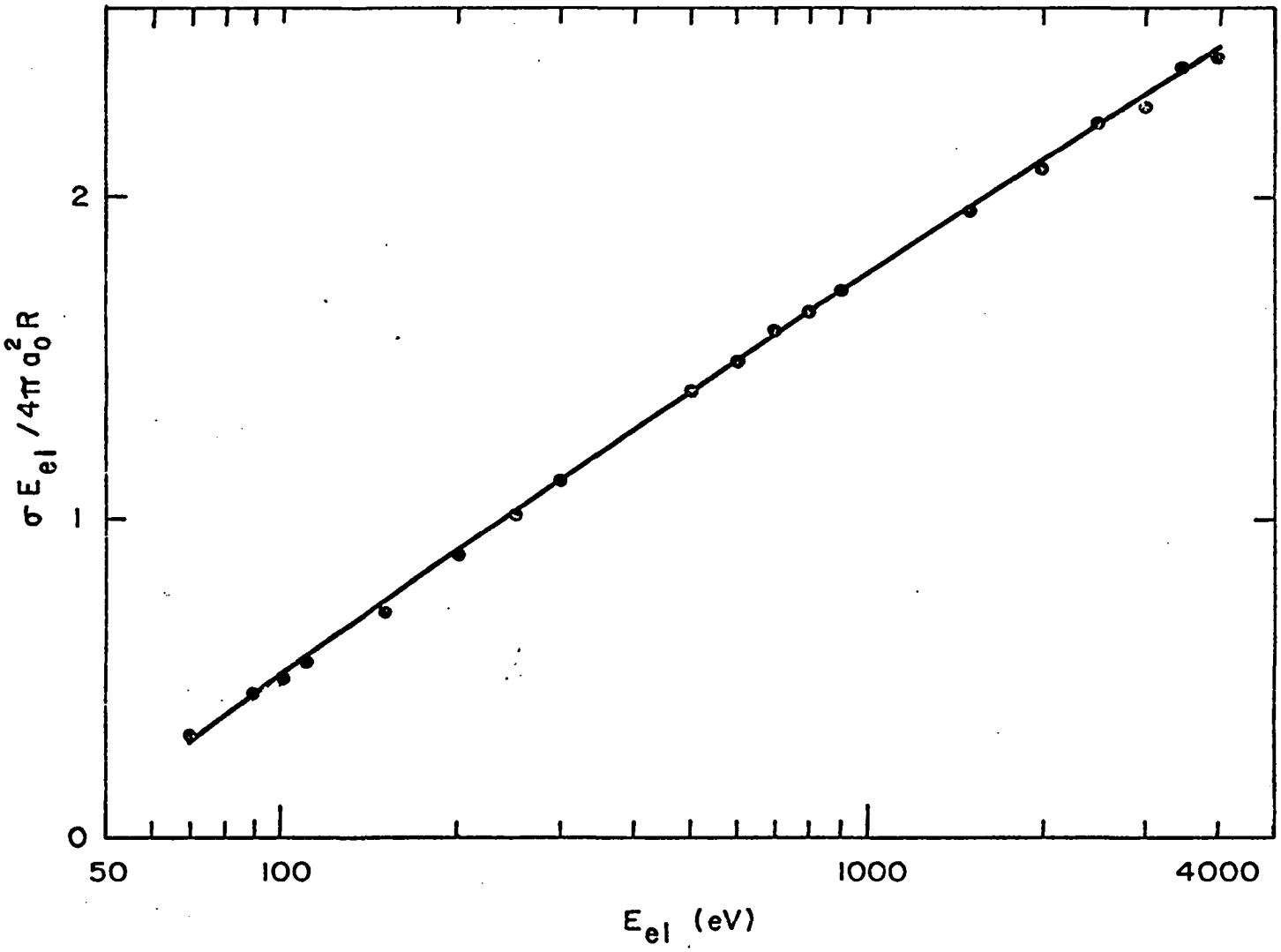

Figure 17 Emission cross sections for v' = 0 vibrational level of N_2^+ B $^2\Sigma_u^+$ plotted as $\sigma E_{el}/4\pi\ a_o^2\ R$ versus ℓn E_{el}.

nicely display an E^{-1} ℓn E variation at the higher beam energies (above 300 eV).

5.2 N_2^+ Meinel Bands

Figure 18 represents the emission cross sections for the (4,1), (2,0) and (3,1) N_2^+ Meinel bands which are also shown in Table 9. The maximum of the cross sections occur at about 100 eV and are marked by an asterisk (*) in the table. Each of these points represents an average of about ten data points. The maximum scatter and the day-to-day reproduction were better than 6%. The emission cross sections are uncorrected for the polarization which is less than 2.5% at 100 eV. The mean ratios of the (2,0),(3,1) and (4,1) bands cross sections are 1 : 0.4 : 0.12.

The excitation cross section Q_v of the vibrational levels v = 2, 3 and 4 of the $A\ ^2\Pi_u$ state are calculated from the measured cross sections of the (2,0), (3,1) and (4,1) N_2^+ Meinel bands by the following equation (Nicholls, 1964):

$$Q_v = \frac{\sum_{v''} q_{v'v''}\ \nu^3_{v'v''}}{q_{v'v''}\ \nu^3_{v'v''}}\ Q_{v'v''} \ ,$$

where $Q_{v'v''}$ is the emission cross section of the (v', v") band; $\nu_{v'v''}$ is the v' - v" transition frequency; $q_{v'v''}$ is the Franck-Condon factor for the v' - v" transition (Nicholls, 1961). The calculated excitation cross sections of the vibrational levels v' = 2, 3 and 4 at the maxima (100 eV) are 13.4×10^{-18}, 3.2×10^{-18} and 1.5×10^{-18} cm^2 respectively.

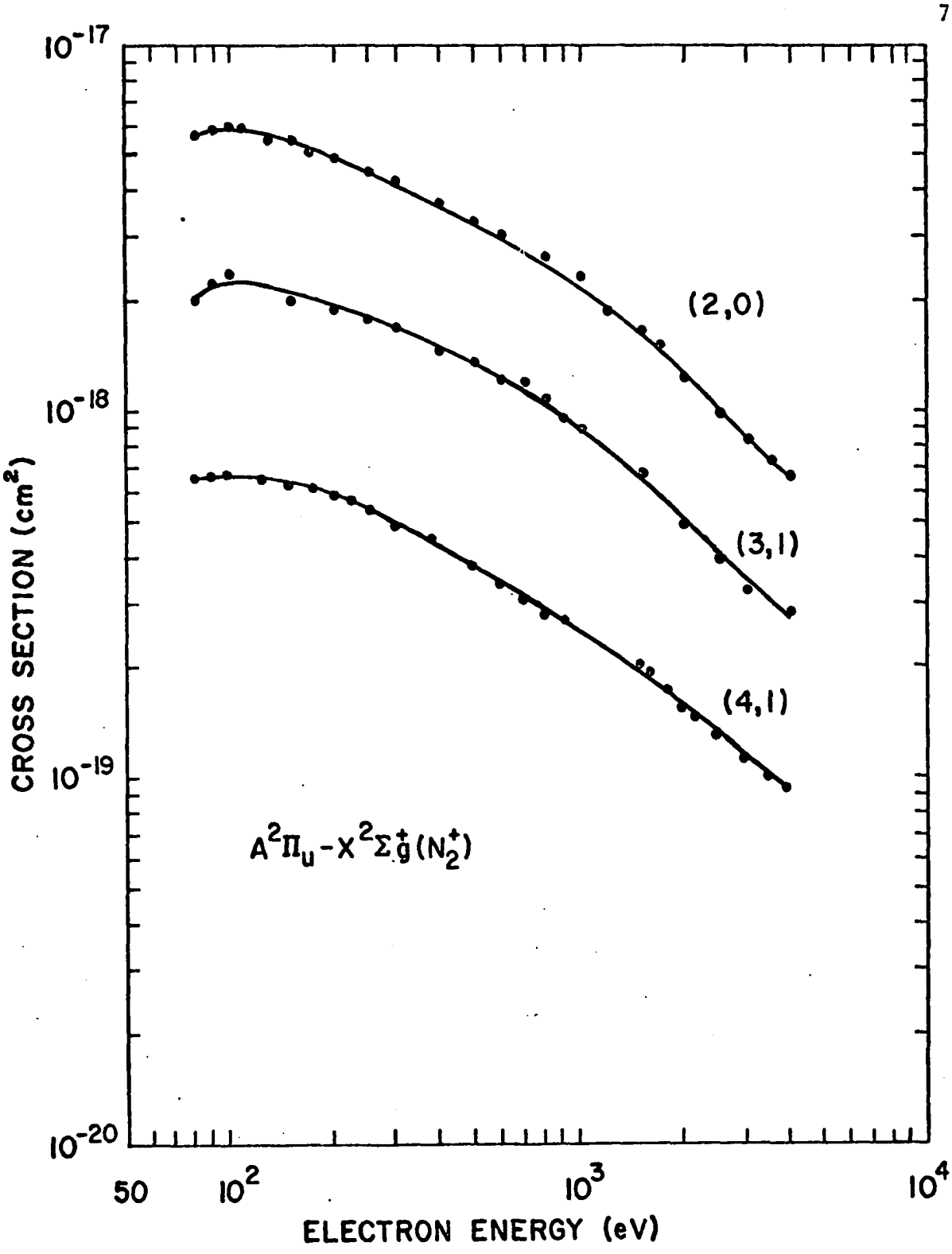

Figure 18 Emission cross sections of N_2^+ Meinel bands produced by electron impact on N_2.

TABLE 9

Emission Cross Sections of N_2^+ Meinel Bands (cm^2)

E	(4,1) (10^{-19})	(2,0) (10^{-18})	(3,1) (10^{-18})
80	6.51	5.62	2.00
90	6.62	5.85	2.21
100	6.76*	6.02*	2.35*
150	6.25	5.50	1.98
200	5.93	4.87	1.88
250	5.37	4.48	1.78
300	4.83	4.20	1.68
500	3.80	3.29	1.37
600	3.35	3.05	1.21
800	2.80	2.67	1.08
1200	2.47	1.86	0.81
1500	2.05	1.68	0.66
2000	1.58	1.23	0.49
2500	1.33	0.99	0.39
3000	1.14	0.83	0.32
3500	1.03	0.72	0.30
4000	0.87	0.68	0.29

5.2.1 Comparison with other Theoretical and Experimental Results

The relative vibrational population obtained from the experimental cross section measurements are compared in Table 10 with those obtained from the Franck-Condon factors of excitation of the A $^2\Pi_u$ state of N_2^+ from the ground state $(X\ ^1\Sigma_g^+)_{v=0}$ of N_2 by electron impact [Nicholls, 1961]. No experimental measurements for the various bands and/or vibrational level excitation cross sections are available for comparison. In determining the vibrational level cross section from the intensity measurement of the single band, the electronic transition moment variation with internuclear separation, the so-called r-centroid, has not been taken into account. This may be one of the reasons for only a fair agreement between theoretical and measured relative populations.

TABLE 10

Relative Vibrational Populations of A $^2\Pi_u$ State of N_2^+

Vibrational Level	Experimental	Theoretical
0	-	1.09
1	-	1.36
2	1.00	1.00
3	0.24	0.55
4	0.11	0.25
5	-	0.11

The total excitation cross section of the A $^2\Pi_u$ state of the Meinel band can be determined using the relative vibrational populations given in Table 10 and the excitation cross section of any vibrational level. Using the excitation cross section of v' = 2 level, the apparent excitation cross section of the A $^2\Pi_u$ state is 5.4 x 10^{-17} cm^2 at 100 eV. This value is in a close agreement with the 4.5 x 10^{-17} cm^2 read from the graph of excitation cross section of the A $^2\Pi_u$ state presented by Skubenich and Zapesochny (1967). However, in the present measurements, the maximum occurs at about 100 eV electron energy whereas Skubenich and Zapesochny (1967) have reported it at about 62 eV.

All available relative intensity measurements of N_2^+ Meinel bands are presented in Table 11. Most of the measurements are from auroral observation. The measurements of Dufay et al. (1966) are for proton impact excitation. The relative intensity of the present measurements are in reasonable agreement with that of the proton impact data.

5.2.2 Comparison with the Total Ionization Cross Sections

The excitation cross sections of the (2,0), (3,1) and (4,1) Meinel bands of N_2^+ are also similar to the excitation cross section of the first negative bands and they are a constant fraction of the total ionization cross section of N_2. The mean fractions are 2.3 x 10^{-2}, 9.0 x 10^{-3}, and 2.7 x 10^{-3}, respectively. The total excitation cross section of the A $^2\Pi_u$ state is nearly 20% of the total ionization cross section of N_2.

The excitation cross section of the N_2^+ Meinel bands can also be represented by means of the Bethe-Born equation for ionization and excitation of the N_2^+ first negative bands. In other words, the measured cross sections display an E^{-1} ℓn E variation at the higher energies.

TABLE 11.

Relative Intensity of N_2^+ Meinel Bands*

Band	Origin λ_o, (μ)	Auroral Measurements					Proton	Electron Impact
		Meinel (1951)	Omholt (1957)	Hunten (1958)	Fedorova (1964)	Brown (1966)	Dufay (1966)	Present Results
0,0	1.11	-	-	-	(35) 51	-	-	
1,0	0,918	-	-	(700)	(100) 147	(100) 131.6	(1000) 208.3	-
2,0	0.785	(105) 100	(78) 100	-	(68) 100	(76) 100	(480) 100	100
2,1	0.947	-	-	(260)	(21) 30.9	(41.2) 54.2	(195) 40.6	-
3,0	0.688	(7) 6.7	(11) 14.1	-	-	(27.7) 36.4	-	-
3,1	0.808	(53) 50.5	(38) 48.7	-	(38) 55.9	(38.5) 50.7	(175) 36.4	39
4,1	0.707	(11) 10.5	(10.3) 13.2	-	-	(27) 35.5	-	13
4,2	0.632	(13) 12.4	(12) 15.4	-	-	(25) 32.9	-	

* The number in parentheses are taken directly from the cited reference; the other figures are normalized to $I_{(2,0)} = 100$

5.3 Experimental Errors

The accuracy of the absolute measurements of the emission cross sections is affected by the following experimental limitations:

(1) Determination of radiant flux: In the visible spectral range, the radiant flux from a tungsten ribbon lamp has associated errors of about ± 5%, allowing for about 2% uncertainty in the emissivity of tungsten.

(2) Gas density measurement: This has been discussed in detail in section 4.6. The estimated error is 5 to 6%.

(3) Polarization of radiation: The determination of the angular distribution of radiation has been described in section 4.4. Since a very small amount of polarization is present, its effects are negligible.

(4) Instrumental polarization: This can cause an error in the measurements. However such an effect was not present in the current measurements. All optical setups were the same during the measurements and calibration.

(5) Nonuniform sensitivity of the photomultiplier surface: The same area of the photocathode was illuminated during calibration and in all measurements and the effect was negligible.

(6) Beam length: The effective beam length is longer than the physical path length due to the streaming of gas as a result of differential pumping. This effective increase in the path length is estimated to be 2%.

(7) Measurement of beam intensities: The electron current and the output of the photometer were integrated and sufficient data points were taken to reduce the counting statistics to better than 1%. The counting accuracy of the scaler is absolute whereas that of the current integrator is 1%.

(8) Impurities in the target gas: Commercially made pre-purified N_2 gas of purity 99.9% was used and this source of error may be negligible.

Therefore, the total estimated error is 15%.

5.4 Fluorescence Efficiency

Available laboratory data indicates that about 35 eV energy is lost in the production of one ion-pair in nitrogen. This energy loss is independent of the energy of the bombarding electrons. [The 35 eV energy loss per ion pair production is based on the measurements at higher electron energies. One should, therefore, be cautious to assume the same value for the energy loss per ion pair production for low energy, less than 100 eV, primary electrons.] The fluorescence efficiency of any band and/or band system can be determined by the following equation

$$\eta_\lambda = \frac{1}{35} \frac{\sigma_{\lambda_{ex}}}{\sigma_{ion}} E_\lambda \ ,$$

where $\sigma_{\lambda_{ex}}$ is the excitation cross section of a particular band λ,

σ_{ion} is the total ionization cross section and E_λ is the energy in eV of the photon. The fluorescence efficiency for the λ3914 band in nitrogen based upon an average value of $\sigma_{3914}/\sigma_{ion}$ from Table 8 is

$$\left(\eta_{3914}\right)_{nitrogen} = 6.15 \times 10^{-3} .$$

Therefore, for an electron beam absorbed in air (80% N_2 and 20% O_2) the λ3914 efficiency is 4.9×10^{-3}. The λ3914 efficiency in air measured by Hartman (1967) is 3.4×10^{-3} for 750 eV electrons. The recent measurements of Hirsh and Poss (1968) indicate a value of $(3.7 \pm 0.5)\ 10^{-3}$ at 1 Kev electron energy.

The estimated value of $\left(\eta_{3914}\right)_{air}$ cannot be given too much weight, since it depends upon the measured values of ionization efficiency and an average ionization cross section, as well as the λ3914 excitation cross sections, all of which have some uncertainty. Also an assumption has been made that the ratio of the number of nitrogen ions to the number of λ3914 photons produced is independent of the energy of exciting electrons over the important energy range. Even so, the above calculated value for $\left(\eta_{3914}\right)_{air}$ is in fair agreement with the efficiency measured in the laboratory. In a way, this may be taken as a confirmation that in the laboratory efficiency experiment each excitation of the parent state of the λ3914 band is produced by a single collision of an electron with N_2 in the ground state.

Similarly, the fluorescence efficiencies of N_2^+ Meinel (2,0), (3,1) and (4,1) bands in air under electron bombardment are 8.3×10^{-4}, 3.2×10^{-4} and 1.1×10^{-4} respectively.

5.5 Excitation of N_2^+ Bands in Aurora

It is certain now, that most auroras are excited by the penetration of energetic electrons in the upper atmosphere. The characteristic energy of these primary electrons lies between 1 keV and 4 keV (Belon, Romick and Rees, 1966) and the electrons lose their energy by ionizing and exciting atmospheric constituents. The N_2^+ first negative emissions result from simultaneous ionization and excitation of N_2. The luminosity of these bands can be related to the incident electron flux and to the rate of ion production by electron impact [cf. Rees (1963) and Dalgarno (1964)].

The photon emission of λ3914 in aurora can be represented by the following expression

$$P_{3914} = \beta\, q(z)\, \frac{n(N_2)_z}{n(M)_z} ,$$

where q(z) is the total ion pair production rate at the atmospheric depth z and depends upon the flux and energy of the incoming particles; $n(M)_z = [n(N_2)_z + n(O_2)_z + \frac{1}{2} n(O)_z]$, [assuming that the total ionization cross section of $O_2 \approx N_2$ and twice the ionization cross section of O atoms (Fite and Brackmann, 1959)]; $n(N_2)_z$, $n(O_2)_z$ and $n(O)_z$ are the density of N_2, O_2 and O atoms, respectively, at the atmospheric depth z, and $\beta = 6.8 \times 10^{-2}$ is a constant which is the ratio of the excitation cross section of λ3914 to the total ionization cross section of N_2.

From the luminosity curve of λ3914 and adopting a model atmosphere, the energy flux of incoming primary electrons can be determined. If the

possibility of large fluxes of soft electrons (with energy less than 1.0 keV) is ignored, the energy flux [ergs cm^{-2} sec^{-1}] in auroras can be determined from the measured photon emission of λ3914 in Rayleighs. In Table 12 the energy fluxes for different IBC auroras are given assuming 70% of N_2 in the atmosphere.

TABLE 12

Energy Flux for Different IBC Auroras

	International Brightness Coefficient			
	I	II	III	IV
Green 5577 line (kR)	1	10	100	1000
λ3914 (kR)	0.5	5	50	500
Energy flux (erg $cm^{-2}sec^{-1}$)	0.6	6	60	600

In section 5.2.2 it has been shown that the $A\ ^2\Pi_u$ upper state of N_2^+ Meinel bands is 20% of the total ionization cross section of N_2. Also the λ3914 (0,0) first negative band of N_2^+ is 6.8% of the total ionization of N_2. Therefore, one should expect that the total Meinel band photon emission in aurora due to electron impact should be 3 times the λ3914 emission. The relative photon emission of both the systems due to electron impact would be insensitive to the change of streaming electron energy distribution function. Chamberlain (1961c) has tabulated intensities of various auroral emissions for an IBC III aurora. The intensity of the λ3914 is 100 kR and of the N_2^+ Meinel bands 2,500 kR. Therefore it seems that a large percentage (88%) of the N_2^+ Meinel bands must be excited by secondary processes.

CHAPTER VI

CONCLUSION

In this chapter the salient features and conclusions of the present study are presented:

The measurements of the excitation cross section of the N_2^+ first negative bands by electron impact have supported the "higher" results of McConkey and Latimer (1965) and are in good agreement with the measurements of Holland (1967). The excitation cross section of (0,0), (0,1) and (0,2) N_2^+ first negative bands have been extended to higher energies (4 keV).

The extension of the Bethe-Born approximation to two electron transitions does not necessarily yield the same results as for the one electron system. In case of ionization and excitation of He as well as dissociative ionization of H_2, a relationship between the cross section and the energy of the beam goes as $\frac{1}{E}$. However, in the case of N_2^+ first negative and Meinel bands, the excitation cross section display $\frac{1}{E}$ ℓn E dependence above electron energies of 300 eV similar to the one electron system.

The excitation cross sections of the N_2^+ first negative and Meinel bands are a constant fraction of the total ionization cross section of N_2.

The relative transition probabilities derived from the experimental results of the cross sections are in good agreement with the theoretical predictions obtained from the Franck-Condon factors.

The estimation of the fluorescence efficiency of the λ3914 (0,0) N_2^+ first negative band, based upon the present emission cross section measurement is in fair agreement with the direct laboratory measurements of Hartman (1967) and Hirsh and Poss (1968).

The energy flux for various types of IBC auroras, estimated on the basis of an average constant ratio (15) between the total ionization cross section and the emission cross section is in accord with the measurements of Belon, Romick and Rees (1966).

The measurements of the absolute emission cross sections of the (4,1), (2,0) and (3,1) N_2^+ Meinel bands by electron impact are the first measurements in the literature. Earlier measurements were only relative or for the $A\ ^2\Pi_u$ upper state of the Meinel system between threshold and 140 eV. The present measurements are from 80 eV to 4.0 keV, the characteristic energy range of the auroral electrons.

The excitation functions of the N_2^+ Meinel bands are similar to the N_2^+ first negative bands. The excitation cross section of the $A\ ^2\Pi_u$ state of N_2^+ is two times the excitation cross section of the $B\ ^2\Sigma_u^+$ state of N_2^+. Semi-empirical calculations of Bauer and Bartky (1965) and Prok et al. (1967) also show that the emission cross section of $A\ ^2\Pi_u$ state of N_2^+ excited by electron impact are 2.2 to 2.5 times the cross section of the $B\ ^2\Sigma_u^+$ state of N_2^+. This is a fair agreement between the experimental result and the semi-theoretical calculations. However, the absolute values of the semi-theoretical cross sections are higher by a factor of three to four than the experimental results.

The intensity estimate for different band systems of N_2^+ in an aurora shows that the total emission from the N_2^+ Meinel bands is 15 to 20 times the total emission of the N_2^+ first negative bands [Chamberlain (1961c), Omholt (1966)] whereas the laboratory measurements by electron impact are only two times the total emission. Therefore, electron impact excitation alone cannot account for the emission of N_2^+ Meinel bands as it can for the N_2^+ first negative bands in aurora. It is apparent that a major portion of the N_2^+ Meinel emissions are due to secondary processes.

A study of the relative intensities of N_2^+ first negative and Meinel bands versus height in different types of aurora will help to uncover the possible excitation mechanism of the N_2^+ Meinel bands.

BIBLIOGRAPHY

Bates, D. R., Relative transition probabilities in band systems of diatomic molecules, Monthly Notices Roy. Astrom. Soc. 112, 614, (1952).

Bauer, E. and C. D. Bartky, Calculation of inelastic electron-molecule cross sections by classical methods, J. Chem. Phys. 43, 2466, (1965).

Belon, A. E., G. J. Romick, M. H. Rees, The energy spectrum of primary auroral electrons determined from auroral luminosity profiles, Planet. Space Sci. 14, 597, (1966).

Brown, M. B., Infrared auroral studies, Master's Thesis, University of Alaska, (1966).

Carr, P. H., Problems in establishing standards for vacuum measurements and in calibrating vacuum gauges, Vacuum 14, 37, (1964).

Chamberlain, J. W., Physics of the Aurora and Airglow, Academic Press, New York, (1961a).

_____, ibid, p. 26, (1961b).

_____, ibid, p. 197, (1961c).

Culp, G. and A. T. Stair, Jr., Effective rotational temperature of N_2^+ (3914Å) excited by monoenergetic electrons in a crossed beam, J. Chimie Physique 1, 57, (1967).

Dahlberg, D. A., D. K. Anderson and I. E. Dayton, Optical emission produced by protons and hydrogen-atom impact on nitrogen, Phys. Rev. 164, 20, (1967).

Dalgarno, A., Corpuscular radiation in the upper atmosphere, Annal. Geophys. 20, 65, (1964).

Dalgarno, A., I. D. Latimer, J. W. McConkey, Corpuscular bombardment and N_2^+ radiation, Planet. Space Sci. 13, 1008, (1965).

Davidson, G. and R. O'Neil, Production of N_2^+ 1N (0,0) radiation by 60 keV electrons, Abstract, IV Intern. Conf. Phys. Electronic and Atomic Collisions, Quebec, p. 428, (1965).

Davidson, G., Comments on "Corpuscular Bombardment and N_2^+ Radiation" by A. Dalgarno, I. D. Latimer and J. W. McConkey, Planet. Space Sci. 14, 651, (1966).

Douglas, A. E., Analysis of the $^2\Pi$ - $^2\Sigma$ bands of the N_2^+ molecule, Astrophys. J. 117, 380, (1953).

Dufay, M., J. Desesquelles, M. Druetta and M. Eidelsberg, Étude de l'excitation de l'azote et de l'oxygène par chocs protoniques, Annal. Geophys. 22, 614, (1966).

Earls, L. T., Intensities in $^2\Pi$ - $^2\Sigma$ transitions in diatomic molecules, Phys. Rev. 48, 423, (1935).

Evans, J. E. and A. E. Belon, Preliminary results from coordinated measurements of auroras, IGY Bull. No. 77, 1, (1963).

Fedorova, N. I., Determining the relative populations of vibrational levels and rotational temperature of the system of bands A $^2\Pi$ - X $^2\Sigma$ of N_2^+, NASA Tech. Translation TT-F-204, Washington, (1964).

Fite, W. L. and R. T. Brackmann, Ionization of atomic oxygen on electron impact, Phys. Rev. 113, 815, (1959).

Hartman, P. L. and H. Hoerlin, Measurements of the fluorescent efficiency of air under electron bombardment, Bull. Am. Phys. Soc. 7, Ser. II, 69, (1962).

Hartman, P. L., New measurements of the fluorescence efficiency of air under electron bombardment, Los Alamos Scientific Laboratory of the Univ. of Calif., LA-3793, (1967).

Hayakawa, S. and H. Nishimura, Measurement of the excitation cross section of N_2^+ first negative band by electron impact, J. Geomag. Geoelect. (Japan) 16, 72, (1964).

Hayakawa, S., T. Kumazaki, H. Nishimura, M. Otsuka, Measurement of the excitation function of N_2^+ first negative bands by electron impact, Rept. Ionosphere Space Res. (Japan) 19, 311, (1965).

Herzberg, G., Über die struktur der negativen stickstoffbanden, Ann. Physik. 86, 189, (1928).

Herzberg, G., Molecular Spectra and Molecular Structure I. Spectra of Diatomic Molecules, D. Van Nostrand Company, Inc., pp. 151, 107, 108, (1950a).

_____, ibid, p. 554, (1950b).

_____, ibid, p. 126, (1950c).

_____, ibid, p. 553, (1950d).

_____, ibid, p. 258, (1950e).

_____, ibid, pp. 168, 169, 232, (1950f).

Holland, P. F., Cross sections for electron excitation of the 3914-Å (0,0) band of the N_2^+ first negative system, Los Alamos Scientific laboratory, Report No. LA-3783, (1967).

Hunten, D. M., Recent work at the University of Saskatchewan on auroral and night sky spectra, Annal. Geophys. 14, 167, (1958).

Jansen, C. G. J. and A. Venema, A McLeod manometer with prescribed volumes for use as a standard instrument, Vacuum 9, 219, (1959).

Kreisman, W. S., Vacuum gauge calibration system, Geophysics Corporation of America, Report No. 61 - 19 - N, (1960).

Mathews, W. G. and L. Wallace, Auroral temperature determination from $A\ ^2\Pi \longrightarrow X\ ^2\Sigma$ bands of the N_2^+ molecule, J. Atmosph. Terrest. Phys. 20, 1, (1961).

McConkey, J. W. and I. D. Latimer, Absolute cross sections for simultaneous ionization and excitation of N_2 by electron impact, Proc. Phys. Soc. (London) 86, 463, (1965).

McConkey, J. W., J. M. Woolsey and D. J. Burns, Absolute cross section for electron impact excitation of 3914Å N_2^+, Planet. Space Sci. 15, 1332, (1967).

McConkey, J. W., D. J. Burns, J. M. Woolsey and F. P. Simpson, Absolute cross sections for electron impact excitation and ionization of atmospheric gases, Abstract, V Intern. Conf. Phys. Electronic and Atomic Collisions, Leningrad, USSR, (1967).

Meinel, A. B., The auroral spectrum from 6200 to 8900Å, Astrophys. J. 113, 583, (1951a).

Meinel, A. B., The analysis of auroral emission bands from the $A\ ^2\Pi$ state of N_2^+, Astrophys. J. 114, 431, (1951b).

Meinke, C. and G. Reich, Vermeidung von Fehlmessungen mit dem System McLeod - Kühlfalle, Vakuum Technik 11, 86, (1962).

Nicholls, R. W., Franck-Condon factors to high vibrational quantum numbers I: N_2 and N_2^+, Journal of Research of the NBS-A, Phys. Chem. 65A, 451, (1961).

Nicholls, R. W., Einstein A coefficients, oscillator strengths and absolute band strengths for the N_2 second positive and N_2^+ first negative systems, J. Atmosph. Terrest. Phys. 25, 218, (1963).

Nicholls, R. W., Transition probabilities of aeronomically important spectra, Annal Geophys. 20, 144, (1964).

Nishimura, H., Excitation of N_2^+, O_2^+, and CO_2^+ band by electron impact, J. Phys. Soc. (Japan) 24, 130, (1968).

O'Brien, B. J. and H. Taylor, High-latitude geophysical studies with satellite injun 3, 4. auroras and their excitation, J. Geophys. Res. 69, 45, (1964).

Omholt, A., The red and near infrared auroral spectrum, J. Atmosph. Terrest. Phys. 10, 320, (1957).

Pearse, R. W. B. and A. G. Gaydon, Identification of Molecular Spectra, 3rd Edition, Chapman & Hall, London, (1963).

Philpot, J. L. and D. H. Hughes, Spectroscopic study of controlled proton impact on molecular nitrogen, Phys. Rev. 133, A107, (1964).

Pillow, M. E., Transition probabilities in band-systems of diatomic molecules: A modified 'distortion' process for the wave functions, Proc. Phys. Soc. (London) A64, 772, (1951).

Podgurski, H. H. and F. N. Davis, A precision McLeod gauge for volumetric gas measurements, Vacuum 10, 377, (1960).

Polyakova, G. N., Y. M. Fogel and A. V. Zats, Rotational and vibrational energy level distributions of N_2^+ ions produced in collisions between electrons and nitrogen molecules, J. Exptl. Theoret. Phys. (U.S.S.R.) 52, 1495, (1967), [English translation: Soviet Phys. JETP 25, 993, (1967).

Prok, G. M., C. F. Monnin and H. J. Hettel, Estimation of electron impact excitation cross sections of molecular hydrogen, NASA Technical Note, NASA TN D-4004, June 1967.

Rapp, D. and P. Englander-Golden, Total cross sections for ionization and attachment in gases by electron impact, I. positive ionization, J. Chem. Phys. 43, 1464, (1965).

Rees, M. H., Auroral ionization and excitation by incident energetic electrons, Planet. Space Sci. 11, 1209, (1963).

Rusch, H. and O. Bunge, Sources of error in pressure measurements with liquid-air trap, Z. Tech. Physik 13, 77, (1932).

Schram, B. L., F. J. DeHeer, M. J. Van der Wiel, J. Kistemaker, Ionization cross sections for electrons (0.6 - 20 keV) in noble and diatomic gases, Physica 31, 94, (1965).

Schram, B. L., H. P. Moustafa, J. Schutten, F. J. DeHeer, Ionization cross sections for electrons (100 - 600 eV) in noble and diatomic gases, Physica 32, 734, (1966).

Shemansky, D. E., Excitation of the N_2 first positive system in the aurora, Ph.D. Dissertation, University of Saskatchewan, Saskatoon, Canada, (1966).

Sheridan, J. R. and K. C. Clark, Vibration and rotation of N_2^+ excited by 10-65 keV ions, Phys. Rev. 140, A1033, (1965).

Sheridan, W. F., O. Oldenberg, N. P. Carleton, Excitation of nitrogen by controlled proton and electron impact, Abstract, II Intern. Conf. Phys. Electronic and Atomic Collisions, Boulder, p. 159, (1961).

Skubenich, V. V. and I. P. Zapesochny, Abstract, V Intern. Conf. Phys. Electronic and Atomic Collisions, Leningrad, USSR, p. 570, July 17-23, (1967).

Srivastava, B. N. and I. M. Mirza, Some results of investigation of the absolute cross sections from simultaneous ionization and excitation of N_2 by electron impact, Trans. Am. Geophys. Un. 48, 73, (1967).

Stair, R., R. G. Johnston and E. W. Halbach, Standard of spectral radiance for the region of 0.25 to 2.6 microns, J. Res. Natl. Bur. Std. 64A, 291, (1960).

Stewart, D. T., Electron excitation functions of infrared nitrogen spectra, Proc. Phys. Soc. (London) A68, 404, (1955).

Stewart, D. T., Electron excitation functions of the first negative bands of N_2^+, Proc. Phys. Soc. (London) A69, 437, (1956).

Tate, J. T. and P. T. Smith, The efficiencies of ionization and ionization potentials of various gases under electron impact, Phys. Rev. 39, 270, (1932).

Wallace, L. V. and R. W. Nicholls, The interpretation of intensity distributions in the N_2 second positive and N_2^+ first negative band systems, J. Atmosph. Terrest. Phys. 7, 101, (1955).

Zapesochny, I. P. and V. V. Skubenich, The cross sections for the excitation of molecular nitrogen levels by electron collision, Opt. i Spektrosk. (USSR) 21, 140, (1966), [English Translation: Opt. Spectrosc. 21, 83, (1966).